Redox Biology 70 (2024) 103011

Contents lists available at ScienceDirect

Redox Biology

journal homepage: www.elsevier.com/locate/redox

Thiol starvation triggers melanoma state switching in an ATF4 and NRF2-dependent manner

Madlen Meinert [a], Christina Jessen [b], Anita Hufnagel [b], Julia Katharina Charlotte Kreß [b], Mychal Burnworth [b], Theo Däubler [b], Till Gallasch [b], Thamara Nishida Xavier da Silva [c], Ancély Ferreira dos Santos [c], Carsten Patrick Ade [d], Werner Schmitz [d], Susanne Kneitz [e], José Pedro Friedmann Angeli [c], Svenja Meierjohann [a,b,f,*]

[a] Department of Physiological Chemistry, University of Würzburg, Würzburg, Germany
[b] Institute of Pathology, University of Würzburg, Würzburg, Germany
[c] Rudolf-Virchow Center for Integrative and Translational Bioimaging, University of Würzburg, Würzburg, Germany
[d] Department of Biochemistry and Molecular Biology, University of Würzburg, Würzburg, Germany
[e] Department of Biochemistry and Cell Biology, University of Würzburg, Würzburg, Germany
[f] Comprehensive Cancer Center Mainfranken, University Hospital Würzburg, Würzburg, Germany

A B S T R A C T

The cystine/glutamate antiporter xCT is an important source of cysteine for cancer cells. Once taken up, cystine is reduced to cysteine and serves as a building block for the synthesis of glutathione, which efficiently protects cells from oxidative damage and prevents ferroptosis. As melanomas are particularly exposed to several sources of oxidative stress, we investigated the biological role of cysteine and glutathione supply by xCT in melanoma. xCT activity was abolished by genetic depletion in the *Tyr::CreER; Braf*^{CA}; *Pten*$^{lox/+}$ melanoma model and by acute cystine withdrawal in melanoma cell lines. Both interventions profoundly impacted melanoma glutathione levels, but they were surprisingly well tolerated by murine melanomas *in vivo* and by most human melanoma cell lines *in vitro*. RNA sequencing of human melanoma cells revealed a strong adaptive upregulation of NRF2 and ATF4 pathways, which orchestrated the compensatory upregulation of genes involved in antioxidant defence and *de novo* cysteine biosynthesis. In addition, the joint activation of ATF4 and NRF2 triggered a phenotypic switch characterized by a reduction of differentiation genes and induction of pro-invasive features, which was also observed after erastin treatment or the inhibition of glutathione synthesis. NRF2 alone was capable of inducing the phenotypic switch in a transient manner. Together, our data show that cystine or glutathione levels regulate the phenotypic plasticity of melanoma cells by elevating ATF4 and NRF2.

1. Introduction

Oxidative stress is a common challenge for melanoma cells during different stages of tumor development [1–3]. During growth and metastasis, human tumors encounter reactive oxygen species (ROS) that originate from the tumor itself (e.g. oncogenes, cellular metabolism) or from exogenous sources (e.g. vasculature, infiltrating immune cells). A well-balanced ratio of oxidants and antioxidants is required to enable the pro-tumorigenic function of ROS and thus prevent their toxic accumulation. Consequently, antioxidant mechanisms are important for tumor viability and metastasis and have been proposed as an Achilles heel of transformed cells [2,4,5].

Cysteine metabolism plays a central role in antioxidant supply, as it gives rise to one of the major thiol-containing cellular antioxidants, glutathione (GSH). GSH is a tripeptide consisting of glutamate, cysteine and glycine and is present intracellularly in millimolar concentrations. GSH biosynthesis is conducted by the consecutive, ATP-dependent enzymatic reactions of glutamyl cysteinyl ligase (GCL) and glutathione synthetase (GSS), where GCL, a dimer consisting of the catalytic (GCLC) and modifier subunits (GCLM), is the rate-limiting step. Functionally, GSH is required as a reducing substrate for various peroxidases and other enzymes involved in the detoxification of toxic electrophilic products or xenobiotics.

GSH production can be limited by substrate availability, particularly glutamate and cysteine. Cancer cells can derive a large fraction of their glutamate demand from exogenous glutamine, which is then metabolized to glutamate by glutaminase; an enzyme frequently upregulated in cancer [6,7]. Cysteine can be supplied via two main routes: import or *de novo* biosynthesis. Within the transsulfuration pathway (TSP), cysteine is synthesized from the essential amino acid methionine. Previous work

* Corresponding author. Institute of Pathology, University of Würzburg, Würzburg, Germany.
E-mail address: svenja.meierjohann@uni-wuerzburg.de (S. Meierjohann).

https://doi.org/10.1016/j.redox.2023.103011
Received 29 November 2023; Received in revised form 20 December 2023; Accepted 21 December 2023
Available online 27 December 2023

by our group showed that an activated TSP allows melanocytes to escape oncogene-induced senescence by preventing the accumulation of aberrant ROS levels [8]. Alternatively, cysteine can be supplied through different import systems, the most prominent being system Xc- (also known as xCT), a cystine/glutamate antiporter composed of a heterodimer of SLC7A11 and its accessory SLC3A2 chain. xCT transports extracellular cysteine in its oxidized form, cystine, in exchange for glutamate [9]. In the cell, cystine is converted to its reduced form by glutathione reductase and thioredoxin reductase [10–12]. In several cancer types, inhibition of xCT was shown to decrease intracellular GSH levels and cause ferroptosis, an iron-dependent form of cell death that is characterized by lipid peroxidation [13]. As the glutathione peroxidase GPX4 is the main enzyme for the detoxification of oxidized membrane lipids, the inhibition of GPX4 by specific inhibitors or by limiting the supply of its cofactor GSH are potent inducers of ferroptosis [14,15]. Generally, inhibitors of the xCT/GSH/GPX4 system fall into two classes of ferroptosis inducers, where class I encompasses GSH depleting compounds and class II contains GPX4 inhibitors [16].

Interestingly, cancer cells with mesenchymal-type features were shown to be particularly sensitive to ferroptosis [17,18]. This observation revealed an important targetable Achilles heel for these tumor subtypes, which are notoriously resistant to targeted therapy [18]. In melanoma, cells with a mesenchymal-type transcriptional signature have low levels of MITF, the melanocytic lineage transcription factor responsible for mediating a proliferative or differentiated phenotype [19]. Consequently, the response of melanoma cells to GPX4 inhibitors or the xCT inhibitor erastin correlates with *MITF* expression [17].

While $MITF^{low}$ melanoma cells readily undergo ferroptosis in response to cysteine deprivation by xCT inhibition, the biological effect of cysteine or glutathione depletion on ferroptosis-resilient cells is largely unknown. Here, we describe the effect of an impaired GSH supply on melanoma cells using an xCT-deficient mouse model and melanoma cell lines kept in absence of an extracellular cystine source. Our data demonstrate that melanoma cells with high or intermediate MITF levels are surprisingly tolerant even to harsh conditions of cystine or GSH depletion, as these lead to a strong activation of the ATF4 and NRF2 pathways enabling the compensatory upregulation of cysteine synthesis and antioxidant pathways. This goes along with a phenotypic switch with pro-invasive features and dedifferentiation.

2. Materials and methods

2.1. In vivo studies

Genetic mouse models were maintained on a C57BL/6J background. The *Tyr::CreERT2; $BRAF^{V600E/wt}$; $Pten^{fl/+}$* melanoma model was previously described [20]. To generate *Tyr::CreERT2; $BRAF^{V600E/wt}$; $Pten^{fl/+}$; $Slc7a11^{-/-}$* mice, *Tyr::CreERT2; $BRAF^{V600E/wt}$; $Pten^{fl/+}$* mice were backcrossed to $Slc7a11^{tm1Hsat}$ mice with constitutive functional *Slc7a11* knockout [21]. To initiate melanoma development, 10 µl of a 1 mM solution 4-hydroxytamoxifen (4-OHT) was applied to the shaved back skin of mice aged 6–8 weeks on three consecutive days, as described previously [20]. Tumor onset was defined as the first timepoint when tumors were clearly palpable (at approximately 4 mm in diameter). Tumor growth was monitored and documented daily. The experiment was terminated when tumor size reached a diameter of 15 mm. All experiments were approved by local authorities (Government of Unterfranken) and were done in accordance with the institution's guidelines.

2.2. Cell culture

M14, SK-MEL-2, UACC-62 and UACC-257 cells are part of the NCI-60 panel and were obtained from NCI/NIH (DCTD Tumor Repository, National Cancer Institute at Frederick, Frederick, Maryland). A375 and SK-MEL-28 were received from ATCC. The doxycycline-inducible UACC-62-NRF2 cell line was previously described. All cells have been authenticated and are regularly tested for contaminations. If not indicated otherwise, cell lines were cultivated in DMEM with 10 % FCS and 1 % penicillin/streptomycin (both from Sigma) at 37 °C and 5 % CO_2. Where indicated, dialysed FCS (Thermo Fisher Scientific) was used. Doxycycline (Sigma) for the inducible expression of ATF4 or NRF2 was applied at indicated concentrations. For generating cystine-free medium, DMEM devoid of methionine, cystine and glutamine (Thermo Fisher Scientific) was used as basal medium, and 1*x* GlutaMax (Thermo Fisher Scientific), 200 µM methionine (Sigma), 10 % FCS and 1 % penicillin/streptomycin were added. As control, this medium was additionally reconstituted with 200 µM cystine (Sigma).

2.3. MTT assay

Cells were seeded in triplicates in a 96-well plate in an equal number. After the indicated treatment with (1*S*, 3*R*)-RSL-3 (Selleckchem) or trametinib (Selleckchem), 5 mg/ml MTT (3-(4,5-dimethylthiazol-2-yl)-2,5-diphenyltetrazolium bromide) was added (1:5) to the cells for 2 h. Afterwards, cells were lysed with 100 µl DMSO. Analysis of the developed formazan accumulation was performed according to the manufacturer's instruction (Sigma).

2.4. Proliferation assay

Cells were seeded in duplicates or triplicates in 6-well plates and treated as indicated. On the respective days, cells were harvested by trypsinization, resuspended in an adequate amount of PBS and counted using a Neubauer hemacytometer.

2.5. Transwell migration assay

Cells were kept in control medium, medium without cystine or in presence of an inhibitor. After indicated time points, 1.25×10^4 cells in their appropriate medium, containing 2 % FCS were applied to the upper layer of the transwell inlay (BD Falcon Cell Culture Insert, 24-well format, 8.0 µm pore size) and the same medium was placed in the lower well. After 24 h, the medium of the lower well was exchanged by the corresponding medium, containing 10 % FCS to attract the cells in case of M14 cells. Cells were allowed to migrate for 8 h or, in case of UACC-62 cells, 16 h. Then, non-migrated cells of the upper layer were removed and migrated cells of the lower layer of the membrane were fixed with ice-cold methanol and stained with 2 % crystal violet. Membranes were washed with PBS and embedded on object slides. Membranes were imaged with a microscope and thereafter, cells were counted.

2.6. Matrigel invasion assay

Cells were pretreated as indicated. Next, 2.5×10^4 cells in their corresponding medium, containing 2 % FCS were applied to the upper layer of the transwell inlay (BioCoatTM Matrigel Invasion Chamber, Corning, 24-well format, 8.0 µm pore size) and the same medium was placed in the lower well. On the next day, medium of the lower well was exchanged by the appropriate medium, containing 10 % FCS to attract the cells. Cells were allowed to invade for 22 h. Afterwards, non-invaded cells and matrigel of the upper layer were removed and invaded and migrated cells on the lower layer of the membrane were fixed with ice-cold methanol and stained with 2 % crystal violet. Membranes were washed with PBS, investigated by microscope and quantified.

2.7. siRNA transfection

80 % confluent melanoma cells in 6 cm dish were treated with either siRNA against human *FOSL1* (Sigma, identifier SASI_Hs01_00191186 and SASI_Hs02_00339593) or *NFE2L2* (Ambion, identifier ID33475 and ID107967)) as well as control siRNA (Sigma, identifier SIC001).

XtremeGene siRNA transfection reagent (Roche) was applied for transfection according to the manufacturer's instruction. After 24 h, cells were reseeded to new dishes for further experiments.

2.8. CRISPR/Cas9 mediated gene knockout

For CRISPR/Cas9 mediated gene knockout in human and murine melanoma cells, two gRNA constructs each for human *ATF4* were cloned using the vector pU6-(BbsI)CBh-Cas9-T2A-mCherry (Addgene #64324) (cloning primers see Supplementary Table 1). Plasmid DNA of positive clones was isolated and confirmed. Two CRISPR/Cas9 constructs with gRNA targeting region were used for transfection of M14 cells. Cells were then selected using hygromycin (Capricorn) and single cells were picked and reseeded. gDNA was isolated from single clones (QIAmp DNA Mini Kit, Qiagen) and knockout validation was done by PCR using individually designed knockout validation primers targeting the gRNA target region in a target gDNA (Supplementary Table 1). PCR products were sequenced and knockout validation was performed. NRF2 knockout clones were generated as described previously [22].

2.9. Construction of lentiviral expression plasmids, preparation of lentiviral particles and cell transduction

For cloning the *TXNRD1* expression vector, codon-optimized human *TXNRD1* (NM_182729.2) was synthesized by IDT as gBlocks™ and cloned using 5 min TA/Blunt-Zero Cloning Kit (Vazyme #C601). The 3′ UTR region was obtained from genomic DNA from the A375 cell line. The fragments were fused with an overlap extension PCR and cloned into p442-IRES-blast vector using ClonExpress MultiS One Step Cloning Kit (Vazyme #C113). Afterwards, HEK 293T cells were used to produce replication-incompetent lentiviral particles pseudotyped with the ecotropic envelope protein of the murine leukaemia virus (MLV) or the pantropic envelope protein VSV-G. A third-generation lentiviral packaging system consisting of the transfer plasmid, pEcoEnv-IRES-puro (ecotropic particles) or pMD2. G (pantropic particles), pMDLg_pRRE and pRSV_Rev was co-transfected into HEK 293T cells using X-tremeGENE HP DNA Transfection Reagent (Roche) as manufactory guidelines. Viral particle containing cell culture supernatants were harvested 48 h after transfection and used to transduce the cell line of interest by directing incubating cell with HEK293T supernatants filtered through a 0.44 μM membrane.

2.10. Construction of sleeping beauty based expression plasmids and stable transfection

The TXN expression vector was generated by ligating PCR-amplified human TXN (using oligonucleotides hTXN_SfiI_up; GCGGCCTCTGAGGCCATGGTGAAGCAGATCGAGAG and hTXN_SfiI_down; GCGGCCTGACAGGCCTTAGACTAATTCATTAATGGTGGC) into the pSB-bi-puro vector (Addgene #60525) after restriction enzyme digestion with SfiI (New England Biolabs). NRF2- and ATF4 overexpression constructs, using the transposase vector pSB-ET-iE, were described previously [22]. pSB-based expression vectors were co-transfected with the sleeping beauty transposase vector pCMV-(CAT) T7- SB100. For transfection, Fugene HD transfection reagent (Promega) or Lipofectamine 3000 (Invitrogen) was used according to the manufacturer's protocol. Positive cells were selected with 1–2 μg/ml puromycin (Calbiochem/Merck).

2.11. RNA extraction, cDNA synthesis and RT-qPCR

RNA isolation of the cell pellet was performed using TRIzol reagent (Invitrogen) according to the manufacturer's protocol. cDNA synthesis was conducted using the RevertAid First Strand cDNA Synthesis Kit (Thermo Fisher Scientific) and hexamer primers according to the manufacturer's protocol. RT-qPCR was performed and analysed with a Mastercycler ep realplex (Eppendorf) or CFX Connect (Biorad) using SYBR Green reagent. Gene expression was normalised to an appropriate housekeeping gene (*Actb* for mouse cDNA, *ACTB* or *RPS14* for human cDNA) using the ΔΔct method. The sequences of the oligonucleotides are indicated in Supplementary Table 2.

2.12. Protein lysis and western blot

Cells were lysed in lysis buffer (20 mM HEPES pH 7.8; 500 mM NaCl, 5 mM $MgCl_2$, 5 mM KCl; 0.1 % deoxycholate, 0.5 % Nonidet-P40; 10 μg/ml aprotinin; 10 μg/ml leupeptin; 200 μM Na_3VO_4; 1 mM phenylmethanesulphonylfluoride and 100 mM NaF or 50 mM Tris pH 8.0; 50 mM NaCl, 1 % Nonidet-P40, 0,1 % SDS; 0.5 % deoxycholate, 1 mM EDTA with 10 μg/ml aprotinin; 10 μg/ml leupeptin; 200 μM Na_3VO_4; 1 mM phenylmethanesulphonylfluoride and 100 mM NaF). Generally, 40 μg of protein per sample was separated by SDS-PAGE and was analysed by western blotting. Antibodies targeting β-actin (sc-47778), CTH (sc-365381) and CBS (sc-271886) were from Santa Cruz Biotechnology. Antibodies against ATF4 (#11815), TXNRD1 (#15140), TXN (#2429) and FRA1 (#5281) were from Cell Signaling. The NRF2 antibody ([EP1808Y], ab62352) was from Abcam, vinculin antibody (V9131) was from Sigma and the MITF antibody was a gift from C. Goding (Oxford Ludwig Institute, University of Oxford, UK).

2.13. Immunofluorescence

Cells were seeded to be 60 % confluent on glass coverslips in 6-well plates. Cells were washed with PBS and were fixed in 4 % PFA (Sigma) and permeabilized for 10 min in 0.2 % Triton X-100/PBS. Afterwards, samples were washed with 0.1 % Triton X-100/PBS (Roth) and PBS. Subsequently, cells were quenched in 100 mM glycerol/PBS (Roth) and blocked in 1 % BSA/PBS (Serva) for 30 min. Then, cells were incubated with primary antibody (MITF, see above) diluted 1:500 in 1 % BSA/PBS for 1 h. After washing with PBS, coverslips were incubated while covered at room temperature with the secondary antibody AlexaFluor594 goat anti-mouse IgG or AlexaFluor594 goat anti-rabbit IgG (Invitrogen) (1:500 in 1 % BSA/PBS), respectively, for 1 h. After washing with PBS, nuclear counterstaining was performed by incubating with Hoechst 34580 (Invitrogen) (1:10000 in PBS) for 10 min. Afterwards, samples were washed with PBS and distilled water and coverslips were embedded with Mowiol (Sigma) on object slides. Samples were determined by inverted fluorescent microscopy.

2.14. CellRox assay

Cells were seeded in triplicates in a 96-well plate and cultured with or without cystine as indicated. Treatment of cells with H_2O_2 for 30 min prior to CellRox reagent (Invitrogen) served as a positive control. CellRox assay was performed according to the manufacturer's protocol. Immediately afterwards, images and quantifications were done using the Alexa647 and Hoechst channels of the Operetta microscope (PerkinElmer). For the ROS measurement of M14 nt and NRF2-ko cells after cystine depletion, CellRox staining was visualized by inverted microscopy (Leica).

2.15. Tietze assay

2×10^5 cells per sample were seeded and treated as indicated. Whole cell pellet was reconstituted in PBS and 5 % sulfosalicylic acid (SSA; Sigma) in assay buffer (143 mM phosphate buffer, 6.3 mM EDTA, adjusted to pH 7.5) (1:3). To lyse the cells, samples were frozen (−80 °C) and thawed for 3 times. Afterwards, samples were centrifuged (12000 rpm, 4 °C, 15 min). For GSH determination, assay buffer with freshly added 0.34 mM NADPH (Biomol), 6 mM DTNB (Sigma), water and cell lysate or the appropriate GSH concentration (7:1:1:0.5) were added to a 1.5 ml cuvette and incubated for 20 min at room temperature.

Afterwards, reaction was started by adding glutathione reductase (GR; Sigma) (20 U/ml in assay buffer) (0.5:0.95). GSH concentrations were determined by observing the rate of change in absorption at 412 nm in a spectrophotometer. Concentrations of GSH were calculated relative to known standard concentrations and cell number.

2.16. Mass spectrometry

For metabolite analysis, cells were seeded in a 10 cm dish in a specified number and treated as indicated. In case of the serine tracing experiment, cells were incubated in DMEM medium containing the equivalent amount of ^{15}N L-serine (0.4 mM) (NLM-2036; Cambridge Isotope Laboratories) instead of the usual unlabeled L-serine. For harvesting, cells were washed with PBS, briefly put in liquid nitrogen, scraped using 800 μl of a methanol/water mix (6.3:3.7) and transferred into an Eppendorf tube. After adding 0.5 ml chloroform, samples were mixed and centrifuged (15 min 14000 rpm at 4 °C). The upper phase was transferred to a new Eppendorf tube and 400 μl of a methanol/water/chloroform mix (1.07:8.82:0.11) were added. Samples were again mixed and centrifuged. Thereafter, the upper phase was evaporated with nitrogen for 30 min and subsequently dried in the speedvac (Savant).

To determine water-soluble metabolites of tumor tissue, 25 mg of tumor tissue was homogenized in water (1:50) using a homogenizer (Potter S). Homogenate was mixed with 0.1 μM lamivudine in methanol (1:4). Samples were mixed, sonicated, again mixed and centrifuged at full speed for 2 min. In the meantime, SPE columns (Strata C18-E, Phenomenex) were activated with 1 ml of acetonitrile and equilibrated with 1 ml of a methanol/water mix (80:20). Then, supernatant of the samples was transferred to the column and the eluate was dried in the speedvac (Savant). The resulting residues were dissolved in 100 μl acetonitrile/water (25:75). For normalisation of the mass spectrometry data, protein concentration of homogenate was determined using Bradford reagent (Sigma). Mass spectrometry was performed using a QExactive orbitrap mass spectrometer, equipped with a heated electrospray ion source (Thermo Scientific). The sample injection was performed by direct injection at a flow rate of 10 μl/min. To generate the GSH and GSSG calibration data, defined concentrations of GSH or GSSG (0.5, 1.0, 2.0, 4.0 and 8.0 μM) were analysed as described above.

2.17. RNA sequencing

After cultivation of M14 melanoma cells in cystine-depleted or control medium for one week, RNA was isolated using the RNeasy Kit (Qiagen) according to the manufacturer's instruction. RNA quality was determined by the Experion Electrophoresis System (Bio-Rad). 500 ng of total RNA was used for Poly-A + RNA isolation using the NEBNext Poly (A) mRNA Magnetic Isolation Module (NEB). NEBNext Ultra RNA Library Prep Kit for Illumina (NEB) was used for library preparation according to the manufacturer's instructions. DNA libraries were amplified with 12 PCR cycles, using index primers from the NEBNext Multiplex Oligos for Illumina kit (NEB). Library quality and quantity was determined by using the Experion Electrophoresis System (Bio-Rad). Sequencing was done using a NextSeq500 Illumina (NB500931) platform. Afterwards, all data were processed using STAR [https://www.ncbi.nlm.nih.gov/pmc/articles/PMC3530905/], RSEM [https://bmcbioinformatics.biomedcentral.com/articles/10.1186/1471-2105-12-323] and DESeq2 [https://bioconductor.org/packages/3.7/bioc/vignettes/DESeq2/inst/doc/DESeq2.html] software, followed by gene set enrichment analysis (GSEA, BROAD Institute).

SK-MEL-28 cells (expressing pSB-ETiE or pSB-NRF2) were treated as indicated, and RNA was isolated with the RNeasy Kit (Qiagen). RNA quality was checked using a 2100 Bioanalyzer with the RNA 6000 Nano kit (Agilent Technologies). The RIN for all samples was ≥9.6. DNA libraries suitable for sequencing were prepared from 500 ng of total RNA with oligo-dT capture beads for poly-A-mRNA enrichment using the TruSeq Stranded mRNA Library Preparation Kit (Illumina) according to manufacturer's instructions (½ volume). After 14 cycles of PCR amplification, the size distribution of the barcoded DNA libraries was estimated ~310 bp by electrophoresis on Agilent DNA 1000 Bioanalyzer microfluidic chips.

Sequencing of pooled libraries, spiked with 1 % PhiX control library, was performed at 25 million reads/sample in single-read mode with 100 nt read length on the NextSeq 2000 platform (Illumina). Demultiplexed FASTQ files were generated with bcl2fastq2 v2.20.0.422 (Illumina). RNA sequencing data are deposited at the NCBI sequence read archive (SRA) under the ID: PRJNA924985. Murine melanomas from the animal model were harvested and fresh-frozen at the experimental endpoint and were isolated using the RNeasy Kit (Qiagen) according to the manufacturer's instruction. 200 ng total RNA per sample was used for RNA sequencing. RNA custom sequencing libraries generated at least 30 million 100-bp paired-end reads for each sample using DNBSeq technology (BGI Genomics). Reads were cleaned and aligned to *Mus musculus* GRCm39 version 105. Differential gene expression was estimated using the R/bioconductor package DESeq2 [23]. Data were visualized by the Integrative Genomics Viewer [24]. RNA sequencing data of the murine melanoma samples are deposited at the NCBI sequence read archive (SRA) under the ID: PRJNA1026766.

3. Results

3.1. xCT is not required for BRAF/PTEN driven melanoma formation

The cystine-glutamate exchanger xCT is considered to be the main source for intracellular cysteine and is highly active in cells with a high GSH demand [25,26] (Fig. 1A). To test if xCT is required for the development of melanoma, we used the *Tyr::CreER; Braf*^{CA}; *Pten*$^{lox/+}$ mouse model [20] and crossed the mice to a *Slc7a11*$^{-/-}$ genetic background [21]. We then initiated *BRAF*^{V600E} expression and *Pten* deletion in melanocytes by applying 4-OHT to the skin of *Tyr::CreER; Braf*^{CA}; *Pten*$^{lox/+}$ and *Tyr::CreER; Braf*^{CA}; *Pten*$^{lox/+}$; *Slc7a11*$^{-/-}$ mice (Fig. 1B) and monitored tumor development. Irrespective of the presence of xCT, melanomas developed in all animals, and tumor onset was comparable in both groups (Fig. 1C). RNA sequencing traces of the *Slc7a11* coding region from xCT-deficient and xCT-proficient melanomas demonstrated the lack of *Slc7a11* expression in the knockout tumors (Supplementary Fig. 1A). To monitor metabolic differences between the tumors, we performed mass spectrometry of five melanomas from each group and found elevated levels of glutamate in xCT-deficient tumors, in line with the abolished Glu/cystine antiporter activity (Fig. 1D). Interestingly, cysteine levels were decreased, while the levels of the oxidized counterpart cystine (the disulfide form of cysteine) were increased in xCT-ko tumors (Fig. 1D). The analysis of glutathione revealed an increase of reduced GSH and an even stronger increase of oxidized GSSG in xCT-deficient melanomas (Fig. 1E), leading to a reduction in the peak area ratio of GSH versus GSSG (Supplementary Figs. 1B and C). This suggests that the melanomas experience pro-oxidative conditions when cystine import is prevented, while overall thiol levels, represented by cyst(e)ine and glutathione, could be maintained. Cell survival under conditions of xCT deficiency can be compensated by an activation of the transsulfuration pathway (TSP) [8,27]. Accordingly, we found that *Slc7a11*-deficient melanoma cells show strongly elevated levels of the gene cystathionase (*Cth*), which catalyzes the last step of the transsulfuration pathway (Fig. 1F). In summary, xCT is dispensable for melanoma formation and does not affect tumor onset despite its strong impact on the glutathione pathway *in vivo*.

3.2. Effect of acute cystine withdrawal on melanoma cell lines

To better understand how melanoma cells react to acute limited cystine supply, we switched to cell culture systems, where different human melanoma cell lines were kept in cystine-free medium for one week. Surprisingly, in some cell lines the cell growth was not affected

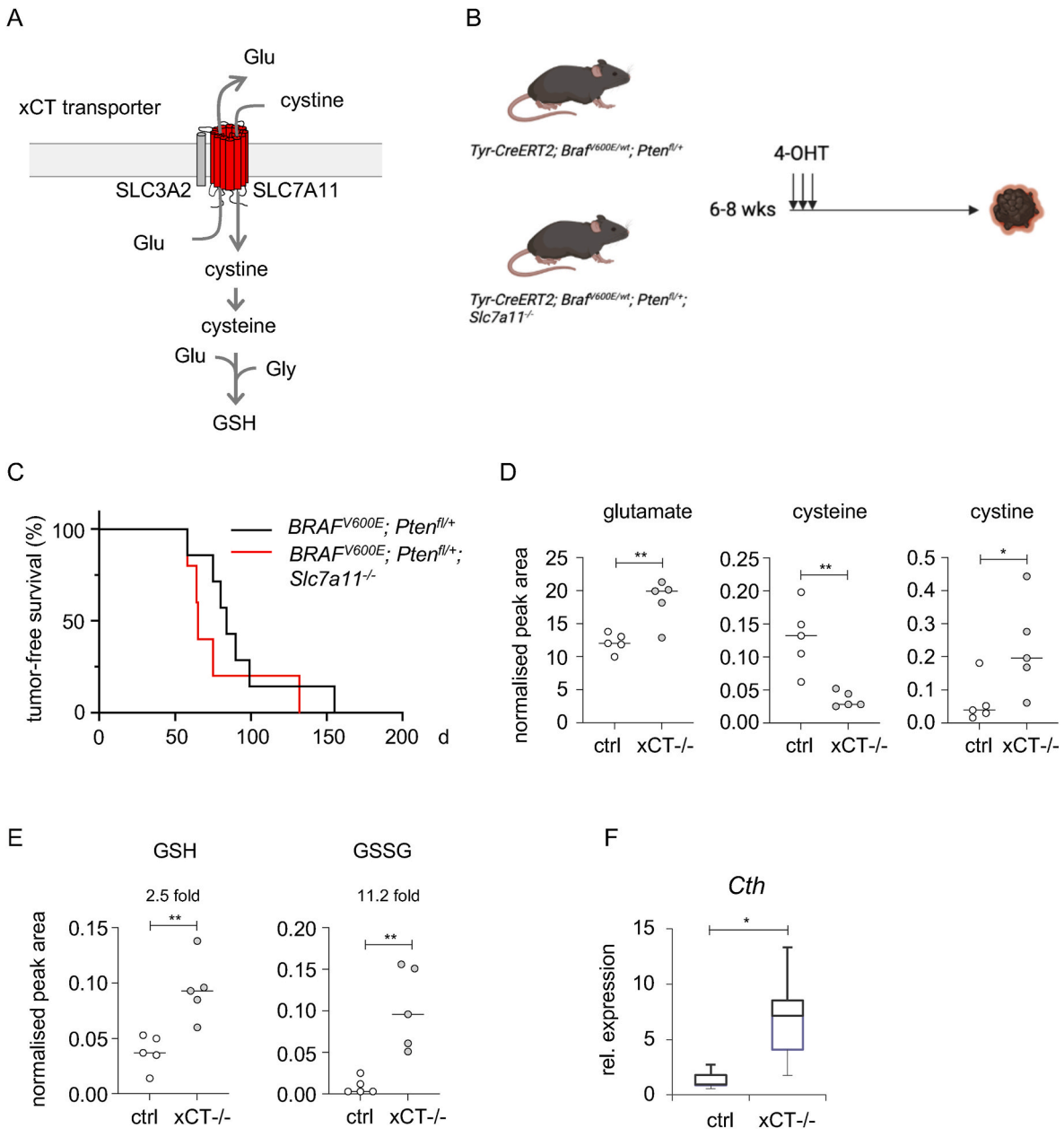

Fig. 1. xCT is dispensable for melanoma formation *in vivo* **A:** Schematic overview of the xCT transporter, importing cystine in exchange for glutamate. xCT is composed of the two subunits SLC7A11 and SLC3A2. Inside the cell, cystine is reduced to cysteine and serves as substrate for GSH synthesis. **B:** Overview of the mouse experiments (created with BioRender). **C:** Kaplan-Meier plot, showing tumor free survival of *Tyr::Cre^{ERT2}; BRAF^{V600E}; Pten$^{fl/+}$* mice in comparison to *Tyr::Cre^{ERT2}; BRAF^{V600E}; Pten$^{fl/+}$; Slc7a11$^{-/-}$* mice. **D:** Corresponding intratumoral levels of glutamate, cysteine and cystine, as measured by mass spectrometry (n = 5 per group). **E:** Corresponding intratumoral levels of GSH and GSSG, as measured by mass spectrometry (n = 5 per group). **F:** RNA expression of *Cth* in tumors from mice in **C**, measured by real-time PCR. Actin served as expression reference. **D-F:** *: $p < 0.05$; **: $p < 0.01$ (Student's *t*-test, unpaired).

(SK-MEL-28, SK-MEL-2), while A375 and UACC-62 were sensitive to the treatment (Fig. 2A). Cell lines M14 and UACC-257 showed an intermediate response with reduced growth, but maintenance of a viable cell population. Notably, the same trend in susceptibility was observed after treatment with the GPX4 inhibitor (1*S*, 3*R*)-RSL3 (Supplementary Fig. 1D) and is in line with the described correlation between ferroptosis sensitivity, MITF activity and differentiation status [17], as A375 and UACC-62 cells express very low MITF levels (Supplementary Fig. 4D). To explore how melanoma cells can cope with cystine depletion, we further analysed M14 cells as representative for a cell line with an intermediate response. The analysis of GSH and GSSG levels revealed that cystine depletion had a massive effect on overall glutathione, which was reduced to levels close to the detection limit (Fig. 2B). In addition, intracellular ROS levels showed an upward trend (Fig. 2C). In order to gain insight into the molecular events triggered by cystine withdrawal, RNA sequencing was performed using M14 cells, which were kept in absence or presence of cystine for 7 days (Supplementary Fig. 2A). The transsulfuration pathway gene *CTH* was among the most strongly upregulated genes (Supplementary Figs. 2A and B) and its induction went along with that of the preceding enzyme in this pathway, cystathionine beta synthase (*CBS*) on RNA and protein level (Fig. 2D and E). Thus, like previously observed in xCT-deficient mice, cystine deprivation *in vitro* leads to the induction of TSP genes. To test if this is accompanied by a functional activation of the TSP, we incubated cystine-starved or control M14 melanoma cells with medium containing isotope-labeled ^{15}N-serine, a substrate of the TSP, and followed its

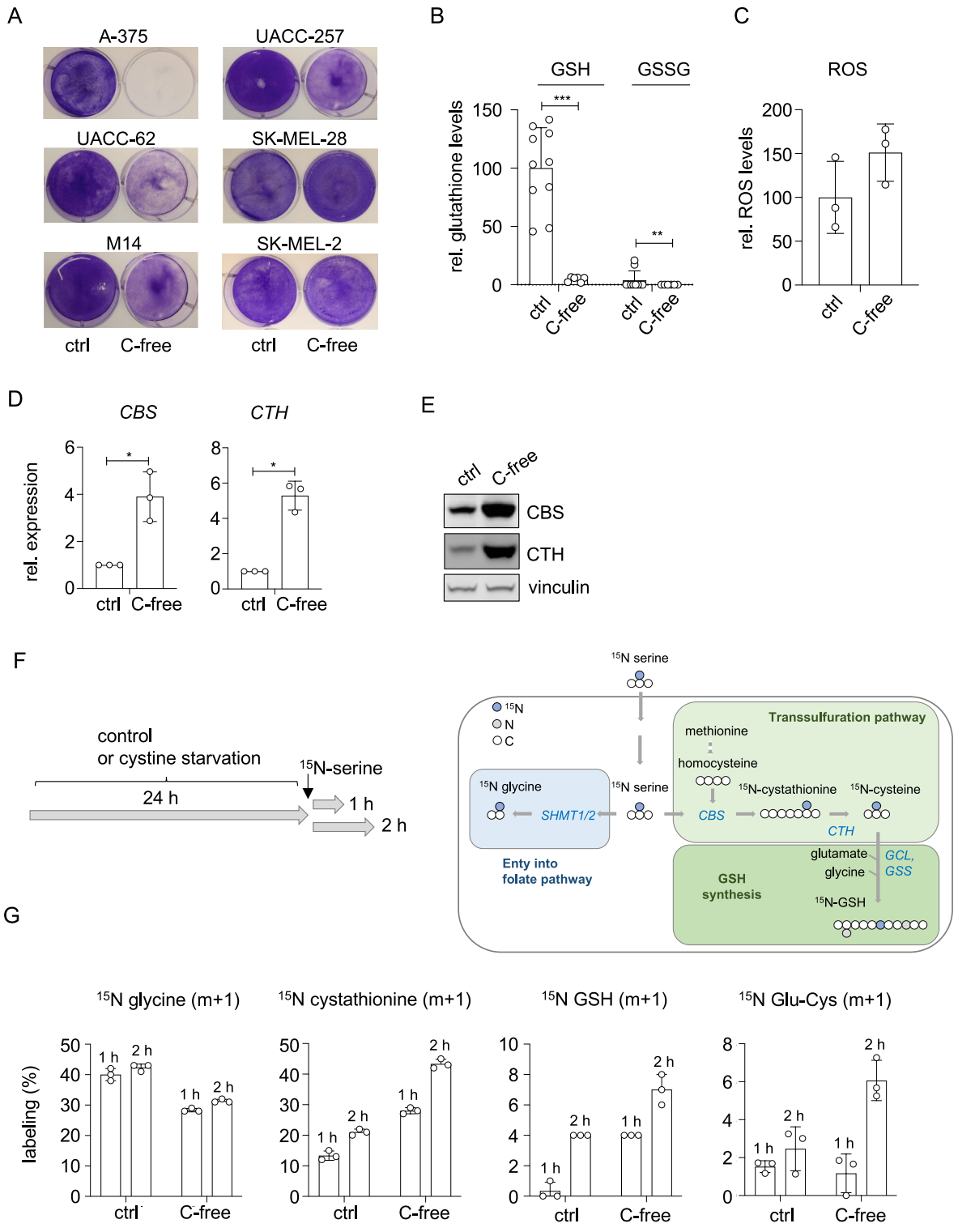

Fig. 2. Activation of the transsulfuration pathway in response to cystine depletion. **A:** Crystal violet staining of indicated melanoma cell lines after cultivation in cystine-free (C-free) or reconstituted (ctrl) medium. **B:** Corresponding GSH and GSSG content in M14 cells, measured by mass spectrometry. $^{**}p < 0.01$, $^{***}p < 0.001$ (unpaired Student's *t*-test). **C:** Corresponding ROS levels in M14 melanoma cells. Cells were stained with CellRox reagent and deep red intensities were measured using the Operetta microscope (n = 3). **D:** RT-qPCR validation of *CBS* and *CTH* in M14 cells after one week of cystine withdrawal (n = 3). $^{*}p < 0.05$, (unpaired Student's *t*-test). **E:** Corresponding western blot analysis of CTH and CBS. Vinculin served as loading control. **F:** Left: Schematic presentation of the metabolic tracing experiment using ^{15}N-serine. Where indicated, cells were kept in cystine depleted or control medium. Right: Overview of the metabolic pathways with incorporated labels derived from ^{15}N-serine. For GSH, all nitrogens are highlighted, with the blue label marking the position of the nitrogen if derived from ^{15}N-cysteine. Alternatively, nitrogens marked in gray may also contribute to ^{15}N GSH (m+1) labeling. **G:** Percentage of ^{15}N-labeled glycine, cystathionine, GSH and Glu-Cys after 1 h or 2 h of ^{15}N serine incubation (n = 3), referred to total levels of the respective metabolite. (For interpretation of the references to colour in this figure legend, the reader is referred to the Web version of this article.)

incorporation into cytosolic metabolites (Fig. 2F). ^{15}N-serine uptake into the cells increased with time and was unaffected by previous cystine starvation (Supplementary Fig. 2C). Serine can be further metabolized to glycine, e.g. in the context of the folate pathway. In cystine-starved cells, ^{15}N-glycine (m+1) production was reduced compared to control cells, whereas the TSP metabolite ^{15}N-cystathionine (m+1) was clearly increased. ^{15}N-cysteine (m+1) was not detectable in the dataset, but we observed a strong increase in ^{15}N-labeled GSH (m+1), particularly in cystine-starved cells (Fig. 2G). Although this does not unequivocally prove the incorporation of newly synthetized ^{15}N cysteine, as ^{15}N GSH (m+1) might also entail ^{15}N label from different serine-derived sources, it shows that glutathione synthesis takes place. This observation is further supported by the increase of ^{15}N Glu-Cys (m+1) in cystine starved melanoma cells (Fig. 2G). Concludingly, these data show that cystine starvation leads to an increased induction of the transsulfuration pathway, as demonstrated by the elevated cystathionine synthesis. Despite undetectable cysteine levels, we show that glutathione is newly synthesized, assuming a contribution of *de novo* generated cysteine.

Next, genes correlating with *CTH* expression in human melanoma cell lines were analysed using the depmap interactive webtool [28]. Both ATF4 and several of its target genes correlated strongly with *CTH* (Fig. 3A). The transcription factor ATF4 is a mediator of the integrated stress response (ISR), which is activated in response to several cellular stress triggers including amino acid starvation and reprograms amino acid metabolism [29]. *CTH* belongs to the *bona fide* target genes of ATF4 [30,31]. In line with this, cystine depletion led to an enrichment of the GO term gene signature "response to starvation", indicative of ATF4 activity, as well as an induction of ATF4 on protein level (Fig. 3B, D). In parallel, the gene set "reactive oxygen species" was identified as second stress pathway strongly affected by cystine starvation (Fig. 3C). Next to *CBS* and *CTH*, this gene set entails genes belonging to several antioxidant pathways that are targets of the transcription factor NRF2. Indeed, NRF2 was induced after cystine starvation (Fig. 3D) and was found to be instrumental for the induction of key antioxidant genes under these conditions (Supplementary Fig. 2D). Concludingly, cystine depletion led to a pronounced activation of the stress-responsive transcription factors ATF4 and NRF2.

3.3. ATF4 and NRF2 enable cell survival after cystine depletion

To test the requirement of ATF4 and NRF2 in the stress response, *ATF4* and *NFE2L2*, the gene encoding NRF2, were knocked out in M14

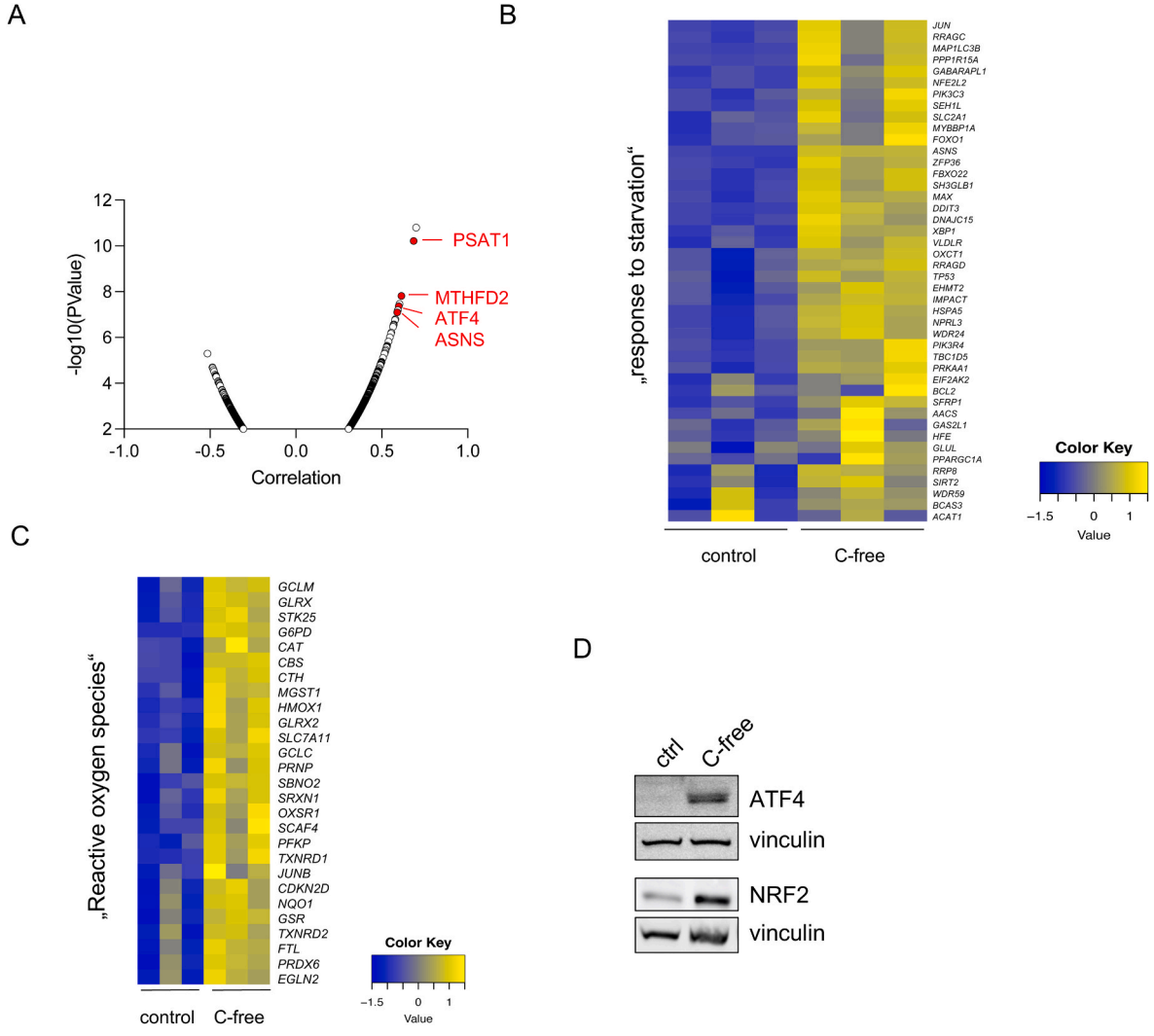

Fig. 3. ATF4 and NRF2 upregulation after cystine depletion. **A:** CTH Pearson correlation analysis, using *CTH* gene expression as dataslice and gene expression 22Q2 public data as dataset from all melanoma CCLE cell lines, as provided by the Cancer Dependency Map (https://depmap.org/portal/; https://depmap.org/portal/ccle/) [28]. **B, C:** Heat plots of the Gene Ontology pathway "response to starvation" **(B)** and the HALLMARK gene set "reactive oxygen species" **(C)** after RNA sequencing of M14 cells treated with control reconstituted or cystine-free medium for 7 days. **D:** Protein blot, showing the expression of ATF4 and NRF2 in whole-cell lysates of M14 cells kept in control reconstituted and cystine-free medium for one week. Vinculin was used as loading control.

cells using CRISPR/Cas9 mediated gene editing. Two independent cell clones were selected for further analyses, respectively. Targeting of *ATF4* led to an incomplete knockout, with clones still expressing residual ATF4, but ATF4 levels were strongly reduced after cystine starvation compared to the controls (Fig. 4B). However, when cultivating ATF4-ko cells under cystine-free conditions, cells died quickly during the first three days, while the control cells only grew at slower rate, as expected (Fig. 4A). We assumed that this might indicate the importance of ATF4 in regulating cysteine availability, as described previously [27]. Indeed, the increase of the TSP genes CBS and CTH that was observed after cystine depletion in control cells was strongly impaired in ATF4-ko cells (Fig. 4B). Inducible ATF4 expression in the melanoma cell line UACC-62 led to a strong induction of CBS and CTH on protein and RNA level (Fig. 4C and D), indicating the dependency of the TSP genes on ATF4.

In addition, the *NFE2L2* knockout was tolerated under control conditions, but became lethal when cells were deprived of cystine (Fig. 4E). Interestingly, slightly reduced CTH levels were also detected in *NFE2L2*-ko cells, although less pronounced compared to ATF4-ko cells (Fig. 4F). Furthermore, the NRF2 targets TXN and TXNRD1, the core components of the cytosolic thioredoxin antioxidant system, were generally lower in *NFE2L2* knockout cells (Fig. 4F). As the thioredoxin pathway becomes particularly important as antioxidant defence system when the GSH pathway is impaired [32], it is likely that an *NFE2L2* knockout oversteps the cellular tolerance of oxidative stress by cystine depletion. Indeed, one day of cystine depletion – a timepoint when *NFE2L2*-ko cells were still viable – resulted in strongly elevated ROS levels in *NFE2L2*-ko cells compared to their controls (Supplementary Fig. 3). The joint overexpression of TXN and TXNRD1 could rescue the viability of *NFE2L2*-ko cells under cystine deprivation (Fig. 4G), revealing their essential roles as NRF2 target genes under these conditions. In conclusion, ATF4 and NRF2 are induced in response to cystine starvation stress to compensate the lack of cysteine and antioxidant defence mechanisms and to enable cellular survival.

3.4. Induction of an invasive signature program in melanoma cells deprived of cystine

Next to the upregulation of stress response pathways, cystine withdrawal induced a group of genes characteristic of "epithelial-mesenchymal transition" (EMT) (Fig. 5A). Different EMT marker genes, including *MMP1*, *MMP3* and *CYR61*, were previously shown to be involved in melanoma invasiveness [33–35] and their upregulation after cystine withdrawal was verified by real-time PCR (Fig. 5B). Analysis of a probe set of 220 phenotypically well-characterized melanoma cell lines [36] revealed a significant enrichment of *MMP1*, *MMP3* and *CYR61* in melanoma cells with invasive phenotype compared to those with proliferative phenotype (Fig. 5C). Accordingly, cystine withdrawal enhanced migration and invasion capacities in M14 cells (Fig. 5D and E). Interestingly, *FOSL1*, the gene encoding the FRA1 protein, was highly upregulated by cystine withdrawal (Supplementary Fig. 2B) and its induction was confirmed on protein level (Fig. 5F). FRA1 is an important mediator of EMT in cancer [37,38] and together with its interaction partner JUN it is strongly linked to a dedifferentiated and pro-invasive state in melanoma [17,39,40]. The stress-induced increase of both migration and invasion was blunted when *FOSL1* was knocked down (Fig. 5G and H), thus showing that FRA1 is involved in mediating the state transition in melanoma cells deprived of cystine.

As an invasive signature in general and the expression of *FOSL1* in particular is inversely correlated to the transcriptional signature guided by the melanocytic lineage transcription factor MITF [41,42], we next investigated the levels of MITF and its pigmentation-relevant target genes *DCT* and *TYR*. MITF was strongly reduced on protein level and was removed from the nucleus under conditions of cystine withdrawal (Fig. 5I and J). In accordance, RNA expression of *MITF*, *DCT* and *TYR* was strongly suppressed (Fig. 5K). Altogether, cystine starvation caused a phenotypic switch, where differentiation features decreased while EMT-like features increased. This phenotypic switch was also observed when cells were cultivated in medium supplemented with dialysed FCS, indicating that cystine introduced by the standard undialysed FCS did not play a role (Supplementary Figs. 4A and B). Furthermore, these changes were detected in several melanoma cell lines, but was more pronounced in cell lines with higher MITF levels and thus a higher differentiation status (Supplementary Figs. 4C–E). The melanoma cell line A375, which harbours already very high FRA1 and extremely low MITF protein levels and maintains pro-invasive characteristics [39], did not show a phenotypic switch (Supplementary Figs. 4D and E), but displayed an ATF4 and NRF2 stress response (Supplementary Fig. 4F). However, while the strength of ATF4 activation, as estimated by upregulation of its target genes, was similar in A375 and the MITF-proficient M14 cell line, NRF2 transcriptional output was much weaker for A375 cells (Supplementary Fig. 4G).

3.5. Glutathione depletion causes transcriptional reprogramming

To provide a better understanding of the involvement of thiol supply in transcriptional reprogramming, several conditions influencing the cysteine and GSH availability and usage were examined. First, it was tested if the alternative cysteine source *N*-acetylcysteine (NAC) counteracts the effects of cystine depletion. The addition of NAC to cystine-deprived medium indeed replenished glutathione levels (Supplementary Fig. 5A) and suppressed the pro-migratory effect as well as the deregulation of differentiation- and invasion-related genes (Supplementary Figs. 5B and C). As cystine supply is directly connected to glutathione levels, we asked if direct glutathione depletion has a similar effect as cystine depletion. For this purpose, buthionine sulfoximine (BSO), an irreversible inhibitor of the glutamyl cysteinyl ligase, which mediates the first step in glutathione synthesis, was used (Fig. 6A). M14 melanoma cells were kept in presence of BSO for 5 days. This led to a strong depletion of glutathione, comparable to the one observed after cystine depletion (Fig. 6B). Similarly, migration (Fig. 6C) and invasion (Fig. 6D) were increased by BSO treatment. This went along with a repression of pigmentation genes and an induction of pro-invasion genes (Supplementary Fig. 6A). When cells were treated for seven days, this effect was further enhanced (Fig. 6E). Like cystine withdrawal, we also observed that the stress-responsive transcription factors ATF4 and NRF2 were elevated after BSO treatment (Fig. 6F, Supplementary Fig. 6B).

Next, inhibitors of the xCT/GSH pathway were investigated. As GSH supply is crucial for the activity of the glutathione peroxidase 4 (GPX4), which is one of the major pathways preventing cell death by ferroptosis [14,15], we also included an inhibitor or GPX4. Inhibition with the xCT inhibitor erastin had a similar effect as cystine depletion, but led to an even stronger induction on ATF4 and NRF2 (Supplementary Fig. 6C). In addition, differentiation genes were efficiently reduced and pro-invasion genes were induced particularly well (Supplementary Figs. 6D and E). In contrast, the GPX4 inhibitor RSL-3 only mildly induced NRF2, but not ATF4, and did not affect the expression of the pro-invasion or differentiation genes (Supplementary Figs. 6C–E).

These data demonstrate that cystine and glutathione depletion, but not GPX4 inhibition, induce an NRF2 and ATF4 emergency response as well as pro-invasion transcriptional reprogramming.

3.6. ATF4 and NRF2 enable the phenotypic switch

It was previously described that the ISR/ATF4 axis suppresses MITF expression and reprograms gene expression towards a pro-invasive state in melanoma [43–45]. To test if this can be confirmed for the marker genes of the phenotypic switch as described in the present study, we used UACC-62 cells, a cell line with basal expression of all chosen indicator genes, but mild development of the phenotypic switch (see Supplementary Figs. 4D and E). UACC-62 cells were transfected with a sleeping beauty control vector (pSB) or the doxycycline-inducible pSB-ATF4 expression vector. To maintain the comparison with the

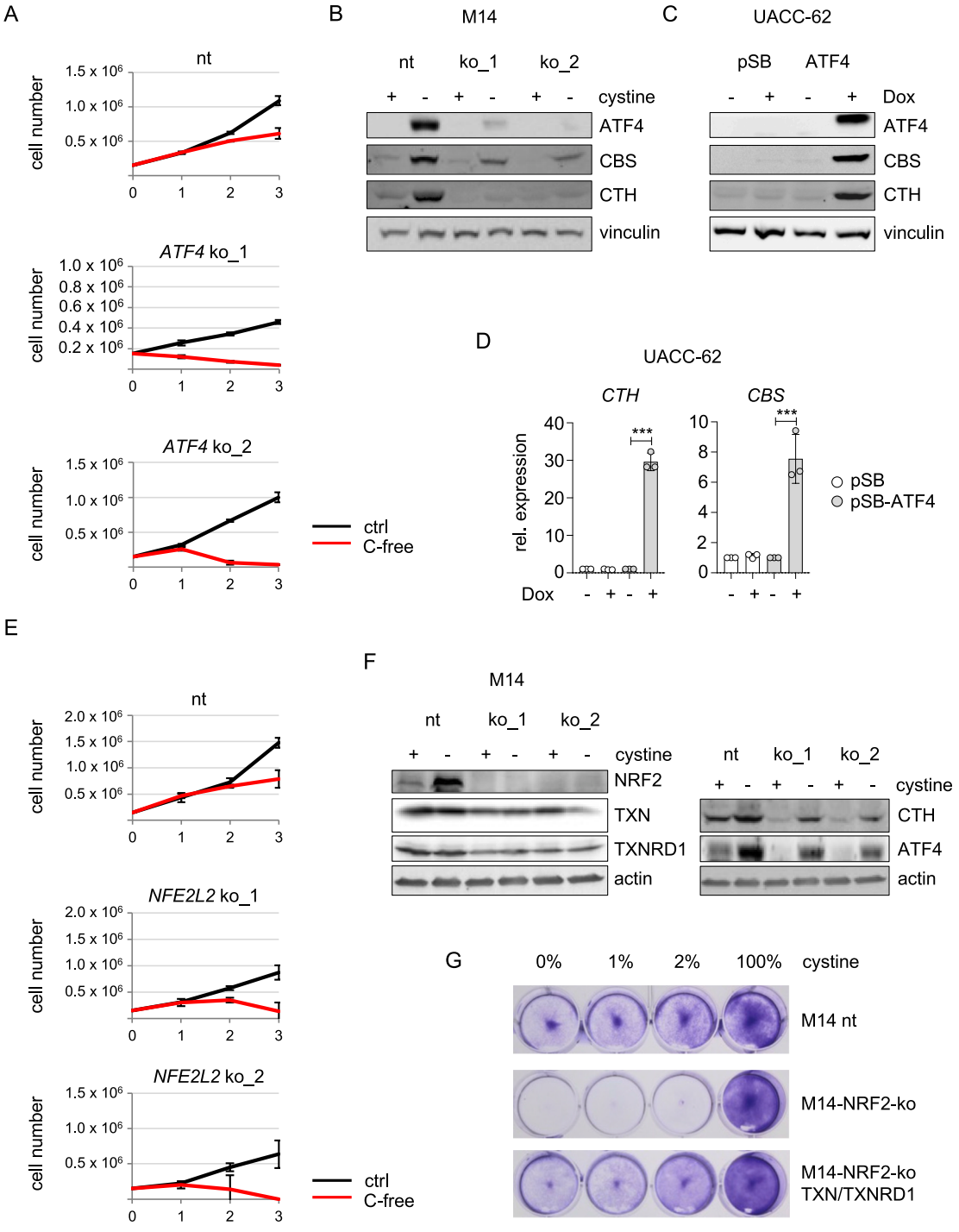

Fig. 4. ATF4 and NRF2 are required for survival in cystine-free medium **A:** Proliferation assay of M14 control cells (nt: non-targeting CRISPR/Cas9 control) and two independent ATF4 knockout clones. Cells were seeded at similar cell numbers, were kept in control (reconstituted) or cystine-free medium and were counted at indicated time points (n = 3). **B:** Protein blot of ATF4 and the transsulfuration pathway proteins CBS and CTH in control and ATF4-ko M14 cells. Where indicated, cells were kept in cystine free medium. Cells were harvested before they exhibited signs of cell death. **C:** Western blot of ATF4, CBS and CTH in UACC-62 cells transfected with control vector (pSB) or an inducible ATF4 expression vector (pSB-ATF4) after incubation with 100 ng/ml doxycycline for 7 days. Vinculin served as loading control. **D:** Corresponding real-time PCR, showing expression of *CBS* and *CTH* (n = 3). ***p < 0.001 (One-way ANOVA with post-hoc Tukey's multiple comparisons test). **E:** Proliferation assay of M14 control cells (nt, see above) and two independent NRF2 knockout clones (equivalent to **A**). **F:** Protein blot of NRF2 and downstream targets TXN, TXNRD1 as well as ATF4 and its downstream target CTH in control and two NRF2-ko M14 cells. Where indicated, cells were kept in cystine free medium. Cells were harvested before they exhibited signs of cell death. **G:** Crystal violet staining of M14 nt cells, NRF2-ko cells or NRF2 ko cells expressing exogenous TXN and TXNRD1. Cells were kept for one week in medium with the indicated cystine concentration before being stained. (For interpretation of the references to colour in this figure legend, the reader is referred to the Web version of this article.)

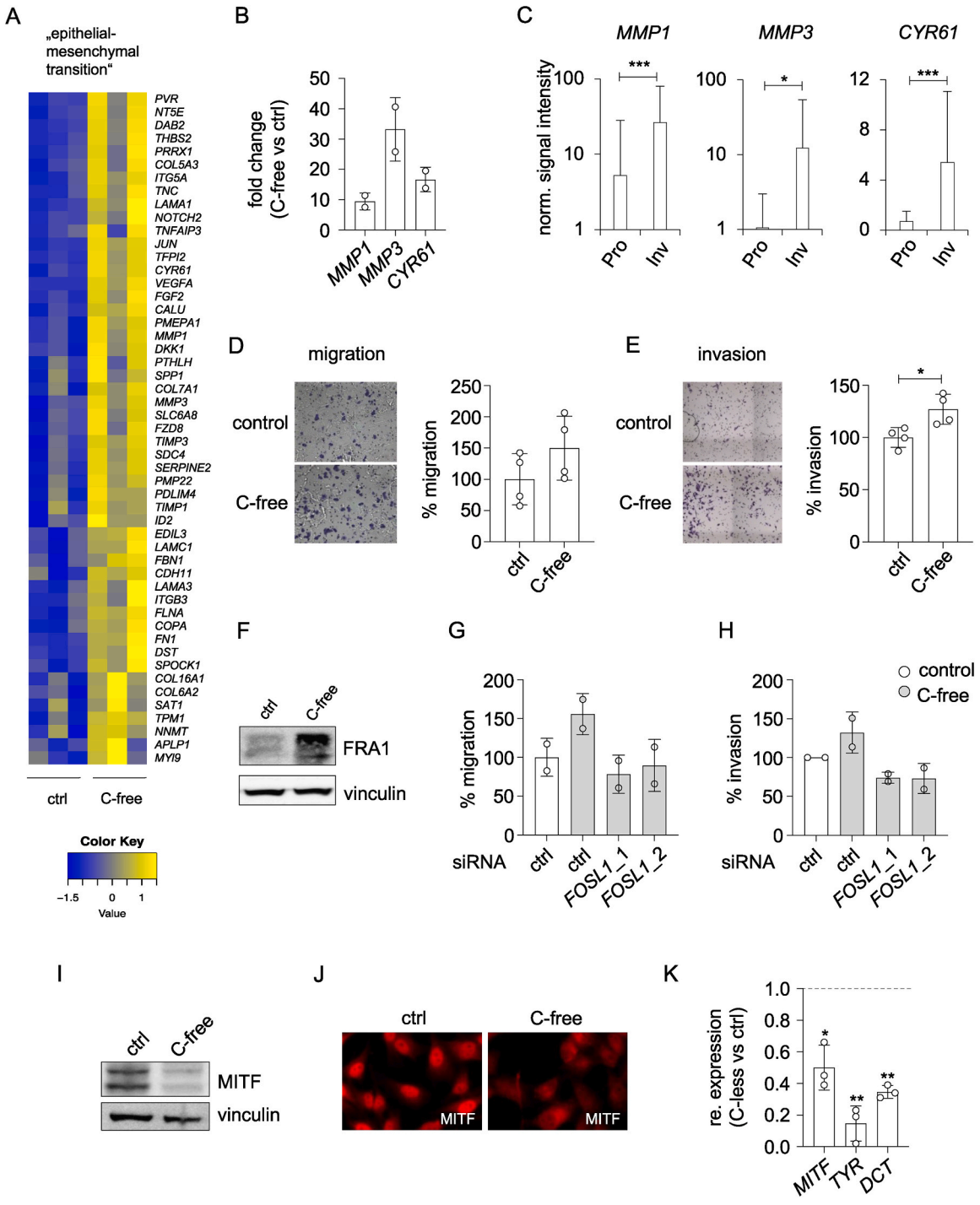

Fig. 5. Cystine depletion causes a phenotypic switch **A:** Heat plot of the HALLMARK gene set "epithelial-mesenchymal transition" in M14 cells treated with control reconstituted or cystine-free medium, derived from the RNA sequencing experiment described in Fig. 3 and Supplementary Fig. 2. **B:** Corresponding real-time PCR of the "EMT" genes *MMP1*, *MMP3* and *CYR61* in M14 cells after 7 days of cystine withdrawal. Cells cultivated in normal medium served as controls and were set as 1. Calculations were made from two individual experiments, each done in triplicates. **C:** Classification of melanoma cells by phenotype-specific *MMP1*, *MMP3* and *CYR61* gene expression according to Widmer et al. [36]. Analysis of a probeset of 220 samples of melanoma cell lines reveals significant expression of these genes in the invasive compared to the proliferative phenotype. *: $p < 0.05$; ***: $p < 0.001$ (Student's *t*-test, unpaired). **D:** Transwell migration assay of M14 melanoma cells in either control or cystine-free medium. Photos were taken (left) and migrated cells were quantified (right) (n = 4). **E:** Matrigel invasion assay of M14 cells in control medium or cystine-free medium. Pictures of invaded cells were taken (left) and quantified (right) (n = 4). *:$p < 0.05$ (Student's *t*-test, unpaired). **F:** Protein blot of FRA1 after one week of cystine withdrawal. Vinculin served as loading control. **G, H:** Transwell migration (**G**) as well as matrigel invasion assay (**H**) after siRNA-mediated knockdown of *FOSL1* in M14 cells, kept in absence of cystine. Counted cells were normalised to control siRNA in control medium. Calculations were made from two experiments. *: $p < 0.05$. **I:** Protein blot of MITF in M14 cells kept in control or cystine-free medium for one week. Vinculin served as loading control. **J:** Corresponding MITF immunofluorescence. **K:** Real-time PCR analysis of *MITF* and its downstream targets *TYR* and *DCT* in M14 cells after 7 days of cystine withdrawal (n = 3). The dashed line indicates the controls, respectively. *:$p < 0.05$, **: $p < 0.01$ (Student's *t*-test, unpaired, gene-wise comparison between controls and cystine-free condition).

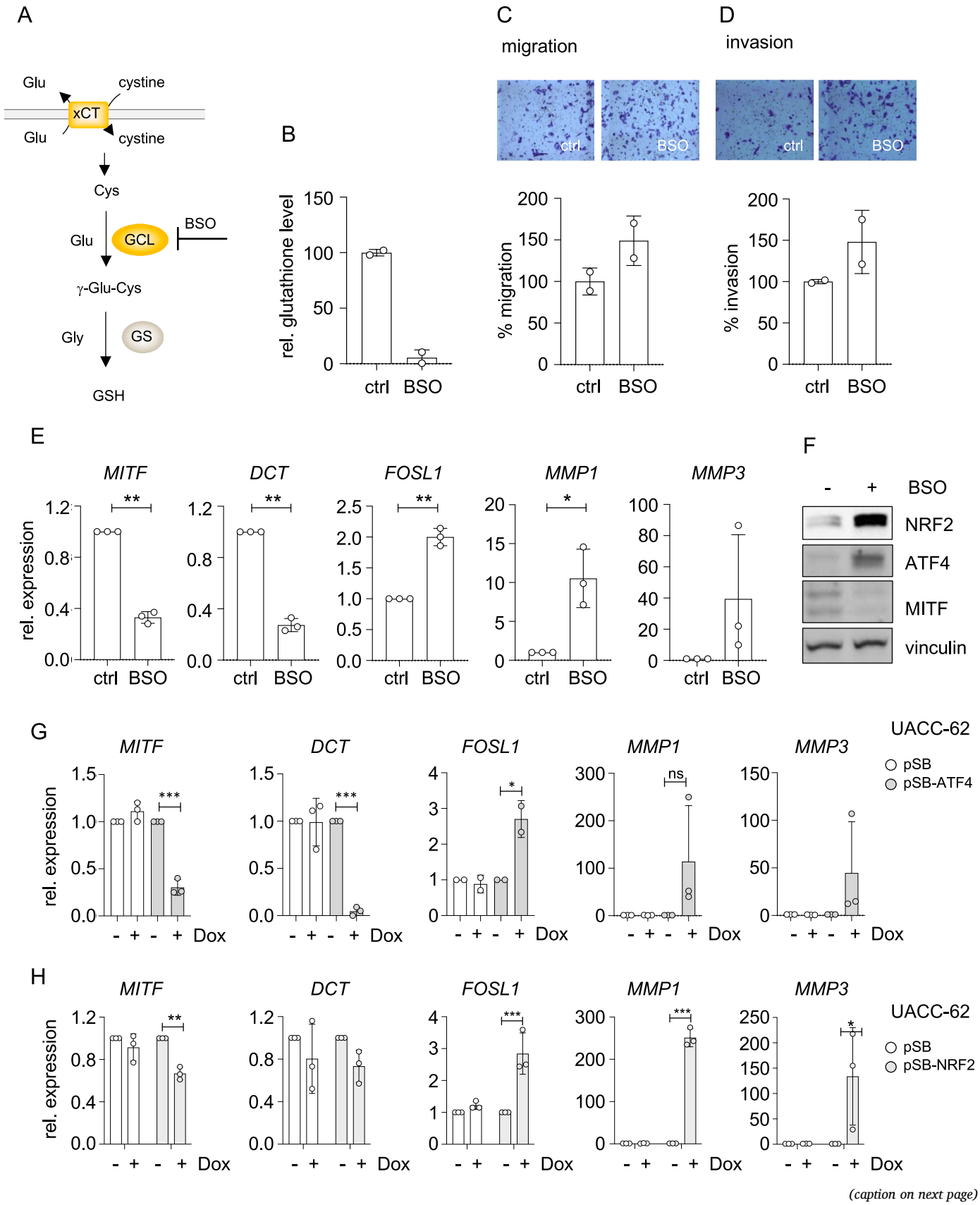

(caption on next page)

Fig. 6. GSH depletion results in phenotypic switch. **A:** Overview of cystine import and glutathione synthesis, the latter being catalyzed by glutamyl cysteinyl ligase (GCL) and glutathione synthetase (GS). GCL is targeted by the inhibitor L-buthionine-(*S*,*R*)-sulfoximine (BSO). **B:** Levels of reduced glutathione, measured by mass spectrometry of M14 cells after 5 days of treatment with BSO (500 μM). Measurements were performed in duplicates. Oxidized glutathione levels were too low to be determined. Glutathione levels were normalised to controls, which were cultivated in parallel in absence of inhibitor. **C:** Transwell migration and **D:** matrigel invasion assay of BSO-treated M14 melanoma cells. After migration or invasion, photos were taken and cells were counted. Counted cells were normalised to untreated M14 cells. Calculations were made from two experiments, each done in duplicates. **E:** RT-qPCR analysis of indicated genes after 7 days of BSO treatment. Gene expression of BSO-treated cells was normalised to control cells. Values were calculated from three independent experiments. Statistical analyses were done using unpaired Student's *t*-test, *: $p < 0.05$, **: $p < 0.0$. **F:** Western blot of NRF2, ATF4 and MITF after 7 days of BSO treatment (500 μM). Vinculin served as loading control. **G:** Real-time PCR of UACC-62 cells transfected with control vector (pSB) or an inducible ATF4 expression vector (pSB-ATF4) after incubation with 100 ng/ml doxycycline for 7 days, showing expression of the genes indicative for the phenotypic switch (n = 2–3). **H:** Real-time PCR of UACC-62 cells transfected with control vector (pSB) or an inducible NRF2 expression vector (pSB-NRF2) after incubation with 500 ng/ml doxycycline for 7 days, showing expression of the genes indicative for the phenotypic switch (n = 3).

extended cystine starvation, ATF4 was also induced for seven days. As expected, this led to a remarkable downregulation of differentiation genes and upregulation of pro-invasive genes (Fig. 6G). Next, it was examined if ATF4 is required for the phenotypic switch in response to thiol depletion. ATF4-knockout melanoma cells do not survive in absence of cystine (Fig. 4A), but they were able to upregulate NRF2 and tolerated longterm inhibition of GSH synthesis by BSO (Supplementary Figs. 7A and B). However, the ATF4 knockout did not affect the suppression of differentiation genes and the induction of pro-invasive genes (Supplementary Fig. 7C), indicating that although ATF4 is capable of inducing the phenotypic switch, it is not required to mediate this effect. As BSO-dependent NRF2 induction was still maintained in ATF4-knockout cells and we previously described a suppressive effect of NRF2 on MITF activity and differentiation [22,46], we asked if NRF2 was also able to mediate the expression of pro-invasive genes and thus acts as trigger for a full phenotypic switch. Dox-inducible NRF2 induction in UACC-62 cells indeed led to a reduction of differentiation markers as well as a profound induction of pro-invasive genes (Fig. 6H, Supplementary Fig. 7D). Because thiol starvation leads to a joint activation of NRF2 and ATF4, we next examined the contribution of NRF2 to the phenotypic switch in the context of activated ATF4. As both cystine depletion and BSO treatment were lethal to NRF2-ko cells (Fig. 4E, Supplementary Fig. 7E), we developed a UACC-62 melanoma cell model that allowed us to induce ATF4 by doxycycline in absence or presence of NRF2 (Supplementary Fig. 7F). After establishing conditions that led to a comparable ATF4 induction in control and NRF2-knockout cells (Supplementary Fig. 7G, labeled in red), ATF4 was induced in both cell lines for one week. Although the NRF2 knockout did not entirely impede the phenotypic switch, it was significantly blunted, as shown by the expression of the majority of indicator genes (Supplementary Fig. 7H). This demonstrates that ATF4 and NRF2 jointly determine the degree of melanoma reprogramming. To address the question if reprogramming is restricted to acute cystine depletion or also applies to the xCT-ko melanoma model - representing durable adaptation - we analysed melanomas from xCT-proficient and xCT-deficient mice (Fig. 1) by protein blot and RNA sequencing. xCT-deficient melanomas showed a trend towards higher ATF4 levels (Supplementary Fig. 8A), which was in accordance with the elevation of the ATF4 target gene *Cth* (Fig. 1F). NRF2 protein levels also showed an upwards trend in xCT−/− melanomas, and *bona fide* NRF2 target genes *Hmox1* and *Gstm2* were increased (Supplementary Figs. 8A and B). Furthermore, GSEA analyses showed an enrichment of EMT genes in the xCT−/− tumors (Supplementary Figs. 8C and D). In summary, signs for reprogramming were also visible *in vivo*. However, metastases were not detected in this mouse model during the duration of the experiment, which was determined by the growth of the primary tumors.

We therefore tested in cell culture, whether the induction of ATF4 and NRF2 in UACC-62 melanoma cells went along with some functional features mediated by EMT-like genes. Indeed, NRF2 induction led to an increased migration capacity (Supplementary Fig. 9A). In case of ATF4, migration was not significantly upregulated, in line with previous observations by Falletta and colleagues [43], assuming that the transcription factor may prime the cells for invasion, but the actual stress input is needed to fully execute it. However, it was described that the EMT-like signature also goes along with resistance against targeted inhibitors (reviewed in Ref. [47]). Thus, we induced either ATF4 or NRF2 in UACC-62 melanoma cells and treated the cells with increasing concentrations of the MEK inhibitor trametinib. Both ATF4 and NRF2 were able to reduce sensitivity towards trametinib (Supplementary Fig. 9B).

3.7. NRF2-dependent reprogramming is dose-dependent and transient

To better understand the nature of NRF2-dependent melanoma reprogramming, bulk RNA sequencing was conducted in SK-MEL-28 cells, a MITF high-expressing cell line with differentiated phenotype [48]. Cells were stably transfected with the inducible NRF2 expression construct pSB-NRF2, and single clones were selected to minimize the impact of cellular heterogeneity. Two different doxycycline concentrations were applied for one week to examine the long term and dose-dependent effects of NRF2. To find out if NRF2 affects melanoma reprogramming in a transient or permanent manner, we furthermore developed conditions for transient NRF2 activation, where the treatment with the higher doxycycline dose was followed by doxycycline withdrawal (Fig. 7A). Although NRF2 went already down to background levels after one day of withdrawal, the one-week withdrawal timepoint was selected in order to ensure sufficient pathway downregulation. In parallel, all conditions were done with the empty vector control (Fig. 7A). GSEA analysis revealed that both the low and the high NRF2 induction led to a profound enrichment of the HALLMARK gene set "epithelial-mesenchymal transition" (EMT), with similar normalised enrichment score (NES). After Dox withdrawal, this signature decreased (Fig. 7B). A side-by-side comparison of NRF2 *bona fide* target genes showed that NRF2 activity was strongly enhanced after low NRF2 activation and increased slightly when NRF2 levels were further elevated. In transiently activated cells, the target genes went back to background levels (Fig. 7C). The same was observed with pro-invasive genes (Fig. 7D), while MITF and other differentiation genes showed the opposite trend (Fig. 7E). Altogether, the data reveal that NRF2 leads to potent transcriptional reprogramming of melanoma, which is coupled to NRF2 activity.

In conclusion, thiol starvation causes the stabilization of ATF4 and NRF2 to enable the maintenance of compensatory pathways such as the transsulfuration and the thioredoxin pathways. This allows melanoma cell survival under stress, but simultaneously leads to a transient pro-invasive phenotype, which is directly caused by ATF4 and NRF2 (summarized in Fig. 7F).

4. Discussion

Here we show that the glutamate-cystine antiporter xCT is dispensable for tumor growth in the $BRAF^{V600E}$/Pten genetic mouse melanoma model. Although signs of oxidative stress such as the elevation of oxidized cystine and GSSG were observed, the tumors maintained considerable overall levels of thiols, suggesting compensatory mechanisms such as the supply of cysteine by other tissues or the melanomas themselves [49,50]. As a result, the growth of the primary tumors was

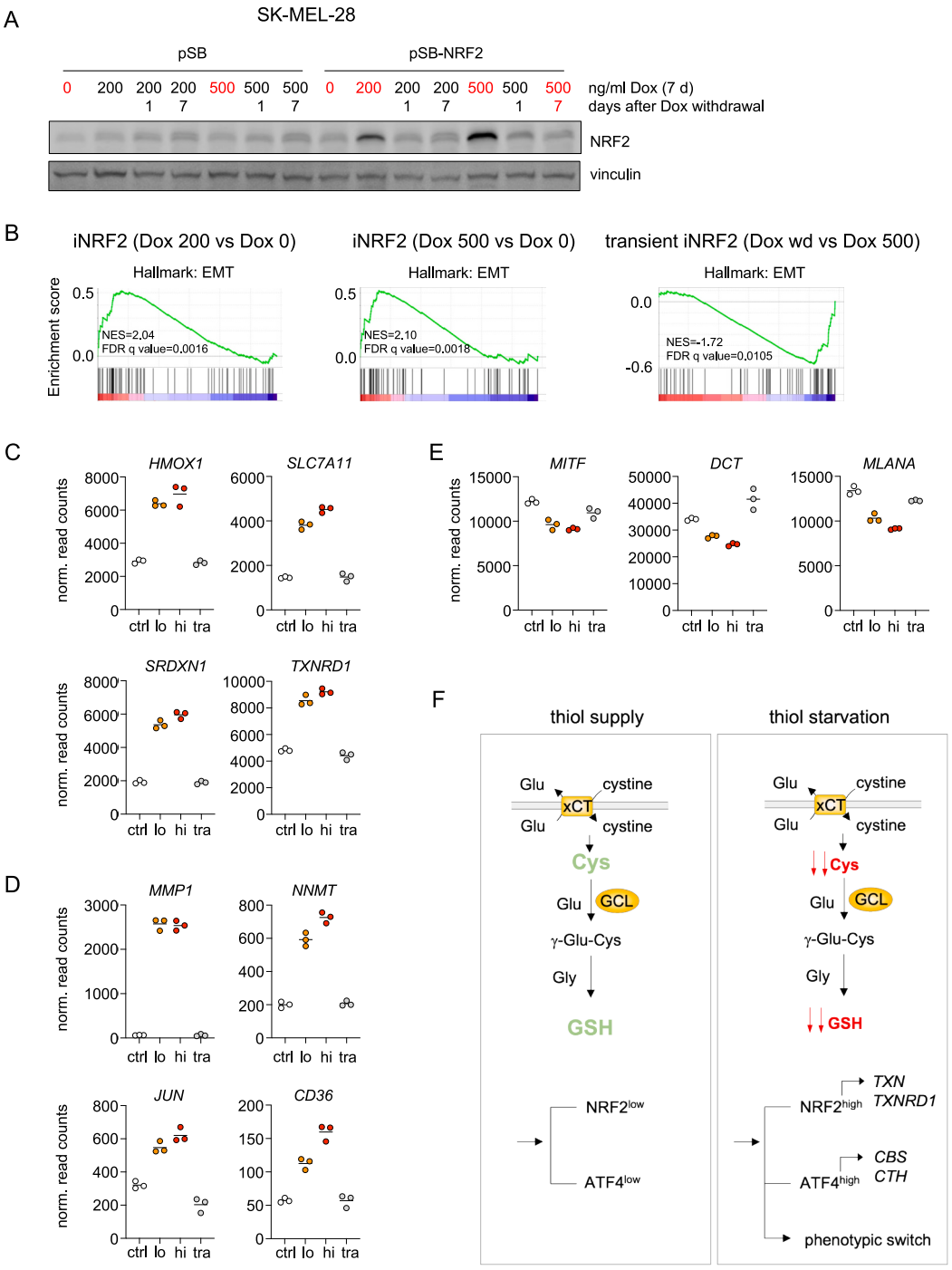

Fig. 7. Transient transcriptional switch by NRF2. **A:** Protein blot of NRF2 in control SK-MEL-28 cells (with pSB control vector) or the Dox-inducible pSB-NRF2 vector (pSB-NRF2, labeled "iNRF2" in the following). Where indicated, doxycycline was added for one week and was subsequently withdrawn for one or seven days. Vinculin served as loading control. Samples marked in red were used for bulk RNA sequencing. **B:** GSEA enrichment plot of the Hallmark gene set "epithelial mesenchymal transition" (EMT). **C-E:** Expression of NRF2 target genes (**C**), EMT genes (**D**) and differentiation genes (**E**) in response to different NRF2 levels as well as transient NRF2 induction. Data show the normalised read counts of RNA sequencing samples from SK-MEL-28 iNRF2 cells in absence of Dox (ctrl), in presence of 200 ng/ml Dox for 7d (lo), in presence of 500 ng/ml Dox for 7d (hi) and after transient treatment with 500 ng/ml Dox (1 week of 500 ng/ml Dox, followed by one week of Dox withdrawal (tra). **F:** Overview of the events caused by thiol depletion. Left: Under conditions of high cysteine and GSH supply, ATF4- and NRF2 levels are low. Right: Thiol depletion leads to a profound upregulation of ATF4 and NRF2, which counteract the cellular stress by enabling cysteine *de novo* synthesis and upregulating the thioredoxin antioxidant system, thereby supporting survival. In addition, ATF4 and NRF2 cause a dedifferentiating phenotypic switch in melanoma. GCL: glutamyl cysteinyl ligase, xCT: glutamate-cystine antiporter; GSH: glutathione, TXN: thioredoxin, TXNRD1: thioredoxin reductase 1, CBS: cystathionine beta synthase, CTH: cystathionase, BSO: buthionine sulfoximine. (For interpretation of the references to colour in this figure legend, the reader is referred to the Web version of this article.)

unaffected. As the mouse model is a complete xCT-knockout, it is likely that the disease outcome is the result of an interplay between xCT-deficient melanoma cells as well as the xCT deficient tumor environment. For example, tumor-promoting cell types such as tumor-associated macrophages and cancer-associated fibroblasts seem to be impaired in absence of xCT, as shown for lung cancer and pancreatic cancer mouse models, respectively [51,52]. In contrast, xCT deletion in T cells had no major effect on the anti-tumor response towards several subcutaneously implanted tumor models, as primary and memory immune responses were maintained [53]. The communication between tumor and environment and the contribution of cancer-associated stroma cell types to the respective tumor growth is therefore important for the tumor outcome under xCT-deficient conditions.

In cell culture, cystine depletion as well as glutathione depletion were also surprisingly well tolerated in most melanoma cell lines due to a profound stress response by the ATF4 and NRF2 transcription factors. As major mediators of genes involved in cysteine supply, glutathione regeneration and antioxidant stress response, ATF4 and particularly NRF2 are well-established factors enabling resistance towards oxidative stress [54–61].

In the present study, both transcription factors were essential for melanoma cell survival under conditions of acute cystine starvation. In contrast, only NRF2 was required for tolerating the inhibition of GSH synthesis, demonstrating the different contributions of ATF4 and NRF2 to intracellular thiol balance. Along with these protective mechanisms, ATF4 and NRF2 are both capable of transferring melanoma cells to a less differentiated, but more invasive state. This reprogramming ability was previously described for ATF4 in melanoma cells [43–45]. We and others furthermore reported that NRF2 suppresses MITF and differentiation in melanoma cells and melanocytes [22,62], but the effect of NRF2 on melanoma plasticity was not previously reported. Our data reveal that ATF4 and NRF2 can independently cause the phenotypic switch in a concentration-dependent manner, demonstrating stress response redundancy. From an evolutionary point of view, this enables cellular migration and invasion independent of the specific stress inducer, thus helping the cells to find their way to a new environment with better nutrient supply. But how does the activation of these two different transcription factors lead to the same phenotypic switch? The explanation might lie in the fact that both inhibit MITF, which was repeatedly demonstrated to suppress genes involved in migration and invasion [48,63]. The fact that we observed a more prominent phenotypic switch in melanoma cells with high MITF is likely due to the fact that the relative change in the expression of differentiation and invasion genes is more pronounced when basal MITF levels are high. However, NRF2 was also connected to mesenchymal features in glioblastoma (GBM), which do not express MITF. Here, SQSTM1/p62 and NRF2 form a positive feedback loop that lead to strongly enhanced NRF2 activity, conveying a mesenchymal phenotype to GBM, which is associated with decreased survival probability [64]. Thus, even in tumor entities that do not show genetic NRF2 activation, durable stress-dependent NRF2 activation is linked to poor outcome.

A limited glutathione availability, mediated by cystine depletion, erastin or BSO, belongs to the major effectors of ferroptosis [65–67]. In melanoma and other solid tumors, ferroptosis sensitivity, e.g. by acute application of erastin or the GPX4 inhibitor RSL-3, seems to depend on the differentiation state, with dedifferentiated (or $MITF^{low}$) melanoma cells being particularly sensitive [17,18,68] – an observation we could confirm in our study. In contrast, melanoma cells with high MITF levels are resistant to ferroptosis inhibitors [17] and, as shown in the present work, tolerated even long times of cystine withdrawal without visible impact on survival or proliferation. It was previously shown that cancer cells with mesenchymal-type gene signature have elevated oxidative stress and lower glutathione levels compared to more differentiated cancer cells [17]. The reasons for this are only partly understood, but it is believed that alterations in cell adhesion, which go along with a pro-invasive phenotype, are accompanied by metabolic reprogramming that result in elevated ROS sensitivity (reviewed in Ref. [69]). Consequently, mesenchymal-type cells quickly undergo cell death in presence of ferroptosis inducers, while differentiated cells are more resilient. This may buy them some time to establish a longer-lasting NRF2- and ATF4 activation, finally enabling their pro-invasive reprogramming.

In summary, our data demonstrate that the depletion of cystine and glutathione, considered classical inducers of ferroptosis, provide MITF-proficient melanoma cells with a pro-invasive ability. Furthermore, our data show for the first time that the pro-oxidant conditions characteristic for mesenchymal cells might rather be a cause than a consequence of the mesenchymal phenotype and are more likely rather connected to a transient cell state than a stable phenotype.

CRediT authorship contribution statement

Madlen Meinert: Formal analysis, Methodology, Visualization, Writing – original draft, Writing – review & editing, Investigation. **Christina Jessen:** Formal analysis, Methodology. **Anita Hufnagel:** Formal analysis. **Julia Katharina Charlotte Kreß:** Formal analysis, Investigation. **Mychal Burnworth:** Formal analysis, Investigation. **Theo Däubler:** Formal analysis, Investigation. **Till Gallasch:** Formal analysis, Investigation. **Thamara Nishida Xavier da Silva:** Methodology, Resources. **Ancély Ferreira dos Santos:** Methodology, Resources. **Carsten Patrick Ade:** Methodology. **Werner Schmitz:** Data curation, Formal analysis, Methodology. **Susanne Kneitz:** Data curation, Methodology. **José Pedro Friedmann Angeli:** Writing – review & editing. **Svenja Meierjohann:** Conceptualization, Funding acquisition, Project administration, Supervision, Visualization, Writing – original draft.

Declaration of competing interest

The authors report no declarations of interest.

Data availability

We have shared the accession link to the data in the Materials and Methods section.

Acknowledgements

This work was supported by the research grants ME1899/4–1 and ME1899/6–1 (German Research Foundation). We thank the Core Unit SysMed at the University of Würzburg for excellent technical support and RNA-seq data generation. The Core Unit was supported by the IZKF at the University of Würzburg (project Z-6). This publication was supported by the Open Access Publication Fund of the University of Wuerzburg.

Appendix A. Supplementary data

Supplementary data to this article can be found online at https://doi.org/10.1016/j.redox.2023.103011.

References

[1] J.M. Ubellacker, A. Tasdogan, V. Ramesh, B. Shen, E.C. Mitchell, M.S. Martin-Sandoval, et al., Lymph protects metastasizing melanoma cells from ferroptosis, Nature 585 (2020) 113–118.
[2] E. Piskounova, M. Agathocleous, M.M. Murphy, Z. Hu, S.E. Huddlestun, Z. Zhao, et al., Oxidative stress inhibits distant metastasis by human melanoma cells, Nature 527 (2015) 186–191.
[3] J.P. Friedmann Angeli, S. Meierjohann, NRF2 dependent stress defence in tumor antioxidant control and immune evasion, Pigment Cell Melanoma Res 34 (2020) 268–279.
[4] C. Gorrini, I.S. Harris, T.W. Mak, Modulation of oxidative stress as an anticancer strategy, Nat. Rev. Drug Discov. 12 (2013) 931–947.
[5] D. Wang, L. Tang, Y. Zhang, G. Ge, X. Jiang, Y. Mo, et al., Regulatory pathways and drugs associated with ferroptosis in tumors, Cell Death Dis. 13 (2022) 544.

[6] M. Momcilovic, S.T. Bailey, J.T. Lee, M.C. Fishbein, C. Magyar, D. Braas, et al., Targeted inhibition of EGFR and glutaminase induces metabolic crisis in EGFR mutant lung cancer, Cell Rep. 18 (2017) 601–610.
[7] E.H. Shroff, L.S. Eberlin, V.M. Dang, A.M. Gouw, M. Gabay, S.J. Adam, et al., MYC oncogene overexpression drives renal cell carcinoma in a mouse model through glutamine metabolism, Proc. Natl. Acad. Sci. U. S. A. 112 (2015) 6539–6544.
[8] C. Leikam, A. Hufnagel, S. Walz, S. Kneitz, A. Fekete, M.J. Muller, et al., Cystathionase mediates senescence evasion in melanocytes and melanoma cells, Oncogene 33 (2014) 771–782.
[9] M. Conrad, H. Sato, The oxidative stress-inducible cystine/glutamate antiporter, system x (c) (-) : cystine supplier and beyond, Amino Acids 42 (2012) 231–246.
[10] P.K. Mandal, A. Seiler, T. Perisic, P. Kolle, A. Banjac Canak, H. Forster, et al., System x(c)- and thioredoxin reductase 1 cooperatively rescue glutathione deficiency, J. Biol. Chem. 285 (2010) 22244–22253.
[11] S.C. Lu, Glutathione synthesis, Biochim. Biophys. Acta 1830 (2013) 3143–3153.
[12] I. Pader, R. Sengupta, M. Cebula, J. Xu, J.O. Lundberg, A. Holmgren, et al., Thioredoxin-related protein of 14 kDa is an efficient L-cystine reductase and S-denitrosylase, Proc. Natl. Acad. Sci. U. S. A. 111 (2014) 6964–6969.
[13] W.S. Yang, B.R. Stockwell, Ferroptosis: death by lipid peroxidation, Trends Cell Biol. 26 (2016) 165–176.
[14] J.P. Friedmann Angeli, M. Schneider, B. Proneth, Y.Y. Tyurina, V.A. Tyurin, V. J. Hammond, et al., Inactivation of the ferroptosis regulator Gpx4 triggers acute renal failure in mice, Nat. Cell Biol. 16 (2014) 1180–1191.
[15] W.S. Yang, R. SriRamaratnam, M.E. Welsch, K. Shimada, R. Skouta, V. S. Viswanathan, et al., Regulation of ferroptotic cancer cell death by GPX4, Cell 156 (2014) 317–331.
[16] B. Hassannia, P. Vandenabeele, T. Vanden Berghe, Targeting ferroptosis to iron out cancer, Cancer Cell 35 (2019) 830–849.
[17] J. Tsoi, L. Robert, K. Paraiso, C. Galvan, K.M. Sheu, J. Lay, et al., Multi-stage differentiation defines melanoma subtypes with differential vulnerability to drug-induced iron-dependent oxidative stress, Cancer Cell 33 (2018), 890-904 e895.
[18] V.S. Viswanathan, M.J. Ryan, H.D. Dhruv, S. Gill, O.M. Eichhoff, B. Seashore-Ludlow, et al., Dependency of a therapy-resistant state of cancer cells on a lipid peroxidase pathway, Nature 547 (2017) 453–457.
[19] C.R. Goding, H. Arnheiter, MITF-the first 25 years, Genes Dev. 33 (2019) 983–1007.
[20] D. Dankort, D.P. Curley, R.A. Cartlidge, B. Nelson, A.N. Karnezis, W.E. Damsky Jr., et al., Braf(V600E) cooperates with Pten loss to induce metastatic melanoma, Nat. Genet. 41 (2009) 544–552.
[21] H. Sato, A. Shiiya, M. Kimata, K. Maebara, M. Tamba, Y. Sakakura, et al., Redox imbalance in cystine/glutamate transporter-deficient mice, J. Biol. Chem. 280 (2005) 37423–37429.
[22] C. Jessen, J.K.C. Kress, A. Baluapuri, A. Hufnagel, W. Schmitz, S. Kneitz, et al., The transcription factor NRF2 enhances melanoma malignancy by blocking differentiation and inducing COX2 expression, Oncogene 39 (2020) 6841–6855.
[23] M.I. Love, W. Huber, S. Anders, Moderated estimation of fold change and dispersion for RNA-seq data with DESeq2, Genome Biol. 15 (2014) 550.
[24] J.T. Robinson, H. Thorvaldsdottir, W. Winckler, M. Guttman, E.S. Lander, G. Getz, et al., Integrative genomics viewer, Nat. Biotechnol. 29 (2011) 24–26.
[25] J.K.M. Lim, A. Delaidelli, S.W. Minaker, H.F. Zhang, M. Colovic, H. Yang, et al., Cystine/glutamate antiporter xCT (SLC7A11) facilitates oncogenic RAS transformation by preserving intracellular redox balance, Proc. Natl. Acad. Sci. U. S. A. 116 (2019) 9433–9442.
[26] A.Y. Shih, H. Erb, X. Sun, S. Toda, P.W. Kalivas, T.H. Murphy, Cystine/glutamate exchange modulates glutathione supply for neuroprotection from oxidative stress and cell proliferation, J. Neurosci. 26 (2006) 10514–10523.
[27] J. Zhu, M. Berisa, S. Schworer, W. Qin, J.R. Cross, C.B. Thompson, Transsulfuration activity can support cell growth upon extracellular cysteine limitation, Cell Metabol. 30 (2019), 865-876 e865.
[28] M. Ghandi, F.W. Huang, J. Jane-Valbuena, G.V. Kryukov, C.C. Lo, E. R. McDonald 3rd, et al., Next-generation characterization of the cancer cell line encyclopedia, Nature 569 (2019) 503–508.
[29] K. Pakos-Zebrucka, I. Koryga, K. Mnich, M. Ljujic, A. Samali, A.M. Gorman, The integrated stress response, EMBO Rep. 17 (2016) 1374–1395.
[30] J.K.C. Kress, C. Jessen, A. Hufnagel, W. Schmitz, T.N. Xavier da Silva, A. Ferreira Dos Santos, et al., The integrated stress response effector ATF4 is an obligatory metabolic activator of NRF2, Cell Rep. 42 (2023) 112724.
[31] J.G. Dickhout, R.E. Carlisle, D.E. Jerome, Z. Mohammed-Ali, H. Jiang, G. Yang, et al., Integrated stress response modulates cellular redox state via induction of cystathionine gamma-lyase: cross-talk between integrated stress response and thiol metabolism, J. Biol. Chem. 287 (2012) 7603–7614.
[32] I.S. Harris, A.E. Treloar, S. Inoue, M. Sasaki, C. Gorrini, K.C. Lee, et al., Glutathione and thioredoxin antioxidant pathways synergize to drive cancer initiation and progression, Cancer Cell 27 (2015) 211–222.
[33] U.B. Hofmann, J.R. Westphal, G.N. Van Muijen, D.J. Ruiter, Matrix metalloproteinases in human melanoma, J. Invest. Dermatol. 115 (2000) 337–344.
[34] S. Ye, S. Dhillon, S.J. Turner, A.C. Bateman, J.M. Theaker, R.M. Pickering, et al., Invasiveness of cutaneous malignant melanoma is influenced by matrix metalloproteinase 1 gene polymorphism, Cancer Res. 61 (2001) 1296–1298.
[35] J. Chen, X. Zhou, J. Yang, Q. Sun, Y. Liu, N. Li, et al., Circ-GLI1 promotes metastasis in melanoma through interacting with p70S6K2 to activate Hedgehog/GLI1 and Wnt/beta-catenin pathways and upregulate Cyr61, Cell Death Dis. 11 (2020) 596.
[36] D.S. Widmer, P.F. Cheng, O.M. Eichhoff, B.C. Belloni, M.C. Zipser, N.C. Schlegel, et al., Systematic classification of melanoma cells by phenotype-specific gene expression mapping, Pigment Cell Melanoma Res 25 (2012) 343–353.
[37] L. Bakiri, S. Macho-Maschler, I. Custic, J. Niemiec, A. Guio-Carrion, S.C. Hasenfuss, et al., Fra-1/AP-1 induces EMT in mammary epithelial cells by modulating Zeb1/2 and TGFbeta expression, Cell Death Differ. 22 (2015) 336–350.
[38] C.J. Desmet, T. Gallenne, A. Prieur, F. Reyal, N.L. Visser, B.S. Wittner, et al., Identification of a pharmacologically tractable Fra-1/ADORA2B axis promoting breast cancer metastasis, Proc. Natl. Acad. Sci. U. S. A. 110 (2013) 5139–5144.
[39] N. Comandante-Lou, D.G. Baumann, M. Fallahi-Sichani, AP-1 transcription factor network explains diverse patterns of cellular plasticity in melanoma cells, Cell Rep. 40 (2022) 111147.
[40] K. Maurus, A. Hufnagel, F. Geiger, S. Graf, C. Berking, A. Heinemann, et al., The AP-1 transcription factor FOSL1 causes melanocyte reprogramming and transformation, Oncogene 36 (2017) 5110–5121.
[41] M. Kunz, H. Loffler-Wirth, M. Dannemann, E. Willscher, G. Doose, J. Kelso, et al., RNA-seq analysis identifies different transcriptomic types and developmental trajectories of primary melanomas, Oncogene 37 (2018) 6136–6151.
[42] S. Riesenberg, A. Groetchen, R. Siddaway, T. Bald, J. Reinhardt, D. Smorra, et al., MITF and c-Jun antagonism interconnects melanoma dedifferentiation with pro-inflammatory cytokine responsiveness and myeloid cell recruitment, Nat. Commun. 6 (2015) 8755.
[43] P. Falletta, L. Sanchez-Del-Campo, J. Chauhan, M. Effern, A. Kenyon, C.J. Kershaw, et al., Translation reprogramming is an evolutionarily conserved driver of phenotypic plasticity and therapeutic resistance in melanoma, Genes Dev. 31 (2017) 18–33.
[44] J. Ferguson, M. Smith, I. Zudaire, C. Wellbrock, I. Arozarena, Glucose availability controls ATF4-mediated MITF suppression to drive melanoma cell growth, Oncotarget 8 (2017) 32946–32959.
[45] Y. Vivas-Garcia, P. Falletta, J. Liebing, P. Louphrasitthiphol, Y. Feng, J. Chauhan, et al., Lineage-restricted regulation of SCD and fatty acid saturation by MITF controls melanoma phenotypic plasticity, Mol. Cell. 77 (2020), 120-137 e129.
[46] J.K.C. Kress, C. Jessen, A. Marquardt, A. Hufnagel, S. Meierjohann, NRF2 enables EGFR signaling in melanoma cells, Int. J. Mol. Sci. 22 (2021).
[47] I. Arozarena, C. Wellbrock, Phenotype plasticity as enabler of melanoma progression and therapy resistance, Nat. Rev. Cancer 19 (2019) 377–391.
[48] R. Dilshat, V. Fock, C. Kenny, I. Gerritsen, R.M.J. Lasseur, J. Travnickova, et al., MITF reprograms the extracellular matrix and focal adhesion in melanoma, Elife 10 (2021).
[49] S. Eriksson, J.R. Prigge, E.A. Talago, E.S. Arner, E.E. Schmidt, Dietary methionine can sustain cytosolic redox homeostasis in the mouse liver, Nat. Commun. 6 (2015) 6479.
[50] S. Mani, G. Yang, R. Wang, A critical life-supporting role for cystathionine gamma-lyase in the absence of dietary cysteine supply, Free Radic. Biol. Med. 50 (2011) 1280–1287.
[51] B. Tang, Y. Wang, W. Xu, J. Zhu, Q. Weng, W. Chen, et al., Macrophage xCT deficiency drives immune activation and boosts responses to immune checkpoint blockade in lung cancer, Cancer Lett. 554 (2023) 216021.
[52] G. Sharbeen, J.A. McCarroll, A. Akerman, C. Kopecky, J. Youkhana, J. Kokkinos, et al., Cancer-associated fibroblasts in pancreatic ductal adenocarcinoma determine response to SLC7A11 inhibition, Cancer Res. 81 (2021) 3461–3479.
[53] M.D. Arensman, X.S. Yang, D.M. Leahy, L. Toral-Barza, M. Mileski, E.C. Rosfjord, et al., Cystine-glutamate antiporter xCT deficiency suppresses tumor growth while preserving antitumor immunity, Proc. Natl. Acad. Sci. U. S. A. 116 (2019) 9533–9542.
[54] N. Takahashi, P. Cho, L.M. Selfors, H.J. Kuiken, R. Kaul, T. Fujiwara, et al., 3D culture models with CRISPR screens reveal hyperactive NRF2 as a prerequisite for spheroid formation via regulation of proliferation and ferroptosis, Mol. Cell. 80 (2020), 828-844 e826.
[55] P. La Rosa, S. Petrillo, R. Turchi, F. Berardinelli, T. Schirinzi, G. Vasco, et al., The Nrf2 induction prevents ferroptosis in Friedreich's Ataxia, Redox Biol. 38 (2021) 101791.
[56] H. Dong, Z. Qiang, D. Chai, J. Peng, Y. Xia, R. Hu, et al., Nrf2 inhibits ferroptosis and protects against acute lung injury due to intestinal ischemia reperfusion via regulating SLC7A11 and HO-1, Aging (Albany NY) 12 (2020) 12943–12959.
[57] N. Liu, X. Lin, C. Huang, Activation of the reverse transsulfuration pathway through NRF2/CBS confers erastin-induced ferroptosis resistance, Br. J. Cancer 122 (2020) 279–292.
[58] M. Gagliardi, D. Cotella, C. Santoro, D. Cora, N.A. Barlev, M. Piacentini, et al., Aldo-keto reductases protect metastatic melanoma from ER stress-independent ferroptosis, Cell Death Dis. 10 (2019) 902.
[59] D. Shin, E.H. Kim, J. Lee, J.L. Roh, Nrf2 inhibition reverses resistance to GPX4 inhibitor-induced ferroptosis in head and neck cancer, Free Radic. Biol. Med. 129 (2018) 454–462.
[60] Y. Wang, Y. Zhao, H. Wang, C. Zhang, M. Wang, Y. Yang, et al., Histone demethylase KDM3B protects against ferroptosis by upregulating SLC7A11, FEBS Open Bio 10 (2020) 637–643.
[61] S. Zhu, Q. Zhang, X. Sun, H.J. Zeh 3rd, M.T. Lotze, R. Kang, et al., HSPA5 regulates ferroptotic cell death in cancer cells, Cancer Res. 77 (2017) 2064–2077.
[62] J.M. Shin, M.Y. Kim, K.C. Sohn, S.Y. Jung, H.E. Lee, J.W. Lim, et al., Nrf2 negatively regulates melanogenesis by modulating PI3K/Akt signaling, PLoS One 9 (2014) e96035.
[63] J. Goodall, S. Carreira, L. Denat, D. Kobi, I. Davidson, P. Nuciforo, et al., Brn-2 represses microphthalmia-associated transcription factor expression and marks a distinct subpopulation of microphthalmia-associated transcription factor-negative melanoma cells, Cancer Res. 68 (2008) 7788–7794.
[64] P. Polonen, A. Jawahar Deen, H.M. Leinonen, H.K. Jyrkkanen, S. Kuosmanen, M. Mononen, et al., Nrf2 and SQSTM1/p62 jointly contribute to mesenchymal transition and invasion in glioblastoma, Oncogene 38 (2019) 7473–7490.

[65] S.J. Dixon, K.M. Lemberg, M.R. Lamprecht, R. Skouta, E.M. Zaitsev, C.E. Gleason, et al., Ferroptosis: an iron-dependent form of nonapoptotic cell death, Cell 149 (2012) 1060–1072.
[66] I. Poursaitidis, X. Wang, T. Crighton, C. Labuschagne, D. Mason, S.L. Cramer, et al., Oncogene-selective sensitivity to synchronous cell death following modulation of the amino acid nutrient cystine, Cell Rep. 18 (2017) 2547–2556.
[67] Y. Sun, Y. Zheng, C. Wang, Y. Liu, Glutathione depletion induces ferroptosis, autophagy, and premature cell senescence in retinal pigment epithelial cells, Cell Death Dis. 9 (2018) 753.
[68] D. Dias, P. Louphrasitthiphol, C.R. Goding, TFE3 promotes ferroptosis in melanoma, Pigment Cell Melanoma Res (2023). https://doi.org/10.1111/pcmr.13149.
[69] N. Ebrahimi, S. Adelian, S. Shakerian, M. Afshinpour, S.R. Chaleshtori, N. Rostami, et al., Crosstalk between ferroptosis and the epithelial-mesenchymal transition: implications for inflammation and cancer therapy, Cytokine Growth Factor Rev. 64 (2022) 33–45.